Molecular Biology of the Cell
Vol. 10, 225–243, January 1999

Disruption of a Dynamin Homologue Affects Endocytosis, Organelle Morphology, and Cytokinesis in *Dictyostelium discoideum*

Dirk C. Wienke,* Menno L.W. Knetsch,* Eva M. Neuhaus,† Mary C. Reedy,‡ and Dietmar J. Manstein*§

*Abteilung Biophysik and †Abteilung Molekulare Zellforschung, Max-Planck-Institut für Medizinische Forschung, D-69120 Heidelberg, Germany; and ‡Department of Cell Biology, Duke University Medical Center, Durham, North Carolina 27710

Submitted May 26, 1998; Accepted October 19, 1998
Monitoring Editor: James A. Spudich

The identification and functional characterization of *Dictyostelium discoideum* dynamin A, a protein composed of 853 amino acids that shares up to 44% sequence identity with other dynamin-related proteins, is described. Dynamin A is present during all stages of *D. discoideum* development and is found predominantly in the cytosolic fraction and in association with endosomal and postlysosomal vacuoles. Overexpression of the protein has no adverse effect on the cells, whereas depletion of dynamin A by gene-targeting techniques leads to multiple and complex phenotypic changes. Cells lacking a functional copy of *dym*A show alterations of mitochondrial, nuclear, and endosomal morphology and a defect in fluid-phase uptake. They also become multinucleated due to a failure to complete normal cytokinesis. These pleiotropic effects of dynamin A depletion can be rescued by complementation with the cloned gene. Morphological studies using cells producing green fluorescent protein-dynamin A revealed that dynamin A associates with punctate cytoplasmic vesicles. Double labeling with vacuolin, a marker of a postlysosomal compartment in *D. discoideum*, showed an almost complete colocalization of vacuolin and dynamin A. Our results suggest that that dynamin A is likely to function in membrane trafficking processes along the endo-lysosomal pathway of *D. discoideum* but not at the plasma membrane.

INTRODUCTION

Dynamins form a protein family within the GTP-binding protein superfamily whose members share considerable sequence identity in the amino-terminal half of the molecule, particularly in the region around the tripartite GTP-binding motif. Large variations in size and sequence are observed in the carboxy-terminal half and are thought to reflect functional differences. Accordingly, members of the dynamin family have been implicated in a wide range of cellular processes, including meiotic spindle pole separation (Yeh *et al.*, 1991), mitochondrial genome maintenance (Jones and Fangman, 1992), cell plate formation in plants (Gu and Verma, 1996), protein trafficking, biogenesis of thylakoid membranes (Park *et al.*, 1998), and various forms of endocytosis. The best characterized function of a dynamin family member, that in clathrin-mediated endocytosis, was deduced from observations in *Drosophila* and mammalian cells. Initial studies of *D. melanogaster shibire* mutants (Kosaka and Ikeda, 1983a,b) and later mammalian cells expressing mutant forms of dynamin (Damke *et al.*, 1994) showed an increase in the presence of invaginations at the plasma membrane. Dynamin-1 localizes to endocytic clathrin-coated pits and self-assembles into rings at the neck of clathrin-coated buds. This process is thought to be a key step in the mechanism by which vesicles are 'pinched off' at the plasma membrane as the dynamin rings constrict (Hinshaw and Schmid, 1995; Takei *et al.*, 1995).

§ Corresponding author.

Many questions remain about the structure and function of dynamins, particularly in regard to a potential role in the organization of the cytoskeleton and the regulation and maintenance of cell shape (Urrutia *et al*., 1997). The present study attempted to identify a dynamin homologue in *Dictyostelium discoideum* and to elucidate its function in this genetically tractable, unicellular organism. These highly motile cells have proven to be a useful system in which to investigate the molecular mechanisms regulating protein and vesicular trafficking along the biosynthetic and endosomal pathways. There is good evidence that many of the components involved in secretion, protein sorting, and endocytosis are well conserved between *D. discoideum* and mammalian cells (Buczynski *et al*., 1997).

We report here the identification, cloning, and characterization of the dynamin-like protein dynamin A from *D. discoideum*. A PCR-based approach was used to identify *dym*A, the gene encoding dynamin A. The functional importance of dynamin A was examined by gene replacement and overexpression of the cloned gene in *D. discoideum.* Disruption of *dym*A causes major changes in the morphology and behavior of *D. discoideum* cells. The mutant cells are large and multinucleated and grow more slowly than wild-type cells. Cells lacking a functional copy of *dym*A show a marked reduction in cell polarity, display aberrant motile behavior, and frequently fail to complete cytokinesis. A role of dynamin A in endocytosis is suggested by the observations that, compared with control cells, the uptake of fluid-phase markers is twofold reduced in *dym*A$^-$ cells and the transit time of the fluid-phase markers is twofold increased. Analysis by electron microscopy revealed extensive areas with small vesicular profiles in *dym*A$^-$ cells and changes in the morphology of mitochondria and the cell nucleus. A causal relationship between the lack of dynamin A and these phenotypic changes was confirmed by complementation of the *dym*A$^-$ cells with the cloned gene. Recovery of *dym*A expression was accompanied by stable reversion to the wild-type phenotype.

MATERIALS AND METHODS

Strains, Media, and Buffers

D. discoideum wild-type and mutant strains were grown on plastic culture dishes or in conical flasks in HL-5c medium. Media for growth of *dym*A$^-$ strains HDM1701, HDM1702, and HDM1703 contained 4 μg/ml blasticidin (ICN Biomedicals, Eschwege, Germany). Buffers used were TBS (20 mM Tris-HCl, 150 mM NaCl, pH 7.5) and PBS (10 mM Na_2HPO_4, 2 mM KH_2PO_4, 137 mM NaCl, pH 7.5). *Escherichia coli* strain XL1-Blue (Stratagene, Heidelberg, Germany) was used for all DNA work unless stated otherwise.

Cloning and Sequencing

The *D. discoideum dym*A gene was cloned using PCR techniques. The oligonucleotide pair used to amplify the dynamin-related sequences, 5′-GATTTCTTACCAGGAGGTTCAGGTAT-3′ and 5′-GCATCIGTACCTTCATCCAT-3′, corresponds to the conserved amino acid sequences DFLPRGSGI and MDEGTDA of human dynamin-1. For the isolation of the cDNA clone, a *D. discoideum* λ-gt11 cDNA library (Clontech, Heidelberg, Germany) was divided into ten fractions made from plates with ~50,000–100,000 plaques. Each fraction was screened using PCR for the appearance of a 0.5-kilobase (kb) fragment. One of the positive fractions was subdivided into eight fractions made from plates with ~15,000 plaques and rescreened. The final λ cDNA clone was isolated by filter screening of a positive fraction using the 500-base pair (bp) PCR fragment as the probe. Standard cloning and DNA hybridization methods were used (Sambrook *et al*., 1989). A genomic clone was isolated to obtain the entire coding sequence of *dym*A. *D. discoideum* genomic DNA was purified from Ax2 cells as described by Manstein *et al*., 1989. Southern blot analysis revealed that a 6- to 7-kb *Hin*dIII–*Eco*RI fragment harbored the complete *Dym*A gene. Consequently a 6- to 7-kb *Hin*dIII–*Eco*RI partial genomic DNA library was created in pBluescript using *E. coli* strain XL2-Blue (Stratagene) as the host, and 1500 colonies were screened with the 500-bp PCR fragment described above. Sequencing confirmed that a 6.6- kb *Hin*dIII–*Eco*RI fragment contained the entire *dym*A gene, and the genomic clone was designated pBS-DYMA. Sequencing was performed using a Sequenase kit (Amersham Buchler, Braunschweig, Germany). Restriction enzymes and T4 DNA ligase were from Boehringer Mannheim (Mannheim, Germany).

Gene Replacement

Plasmid pBS-ΔDYMA was generated for the replacement of the *dym*A gene in *D. discoideum* (Figure 3). First, pBS-DYMA was cut with *Spe*I and religated to obtain pBS-DYMAΔSpe. The 134-bp *Bam*HI–*Eco*RV DNA fragment of pBS-DYMAΔSpe was then replaced by the 1.4-kb blasticidin S resistance cassette from pBsr2 (Sutoh, 1993). The resulting construct (pBS-ΔDYMA) had the blasticidin S resistance cassette inserted 664 bp downstream of the *dym*A start codon and in the same orientation as the *dym*A gene.

For transformation of wild-type Ax2 cells, 20 μg of pBS-ΔDYMA were digested with *Nde*I–*Spe*I to release the replacement fragment from the vector sequence. The DNA was dephosphorylated with shrimp alkaline phosphatase (Amersham Buchler), phenol/chloroform extracted, ethanol precipitated, and resuspended in 20 μl Tris-EDTA, pH 8.0. Alternatively, after digestion with *Nde*I–*Spe*I the replacement fragment was gel purified and resuspended in 20 μl Tris-EDTA, pH 8.0. Transformation of *D. discoideum* cells was carried out as described (De Hostos *et al*., 1991). Selection for transformants was applied 24 h after transformation in medium containing 4 μg/ml blasticidin S. Colonies appeared around day 5. Transformants were picked after 7–10 d and subcloned by spreading series of diluted cell suspensions onto SM agar plates containing *Klebsiella aerogenes*. Transformants were screened by PCR, and the replacement event was verified by Southern blot analysis.

Extrachromosomal Expression of Dynamin A

For complementation studies, the entire *dym*A gene was recovered from plasmid pBS-DYMA as a 6.6-kbp *Sal*I–*Xba*I fragment. This fragment also contained 1.5 kbp of 5′-flanking region including the native promoter of *dym*A. The *Sal*I–*Xba*I fragment was cloned into the *Dictyostelium* expression plasmid pDXA-3C (Manstein *et al*., 1995), cut *Sal*I–*Xba*I thus releasing the actin 15 promoter. The resulting construct (pDX-DYMA) was transformed into *dym*A$^-$ cells, and transformants were selected in growth medium containing 10 μg/ml G418.

Expression of Green Fluorescent Protein (GFP)–Dynamin A

A vector for expression of a GFP–dynamin A fusion protein in *D. discoideum* under the control of the actin 15 promoter was con-

structed from the transformation vector pDEX H (Faix *et al.*, 1992). The insert contained a continuous reading frame composed of, first, the coding sequence of S65T-GFP from *A. victoria* (Heim *et al.*, 1995); second, an oligopeptide linker consisting of four glycine-serine-glycine repeats (Westphal *et al.*, 1997); and third, the entire *dym*A coding sequence. The vector was introduced into the genome of Ax2 cells using electroporation, and transformants were selected in growth medium containing 10 μg/ml G418. The transformant clone HDM1718 was used for morphological studies.

Antibody Production and Western Blot Analysis

A fragment containing amino acids 1–380 was expressed as GST fusion protein and purified on a GST-agarose column. Polyclonal antisera against dynamin A were obtained from rabbits immunized with the GST-fusion protein. Antibodies were affinity purified using a dynamin fragment corresponding to amino acids 1–568 that was CNBr coupled to Sepharose. Eluted antibody was precipitated with 50% NH_4SO_4, resuspended in PBS, and dialyzed overnight at 4°C against PBS. For immunoblotting, *D. discoideum* proteins from wild-type and mutant strains were separated on a 10% SDS-PAGE gel and electroblotted onto nitrocellulose (Schleicher & Schüll, Dassel, Germany). The nitrocellulose blot was blocked in TBS containing 5% nonfat dry milk powder for 1 h, incubated with 1:1000 dilution of affinity-purified anti-dynamin antibody in the same buffer for either 1 h at room temperature or overnight at 4°C followed by detection with an HRP-conjugated secondary antibody (Bio-Rad, Munich, Germany). Detection by ECL was performed according to manufacturer's instructions (Amersham Buchler).

Fluorescence Microscopy

Cells at a density of 1×10^6 cells/ml were placed on 12-mm coverslips and allowed to attach for 30 min. Fixation of cells was performed in methanol applying a temperature gradient from −85 to −35°C for 30 min (Neuhaus *et al.*, 1998). The cells were rehydrated in PBS and blocked in PBS containing 3% BSA followed by incubation in primary antibody for 30 min at room temperature. Immunolocalization of dynamin A used antibody PAD1 at a dilution of 1:20 in PBS containing 3% BSA and 0.1% Triton X-100. For immunostaining of mitochondria, the monoclonal α-mitoporin-antibody 70-100-1 was used (Troll *et al.*, 1992). Other primary antibodies used were monoclonal antibody 190-340-8 (Weiner *et al.*, 1993) to stain the Golgi complex, monoclonal vacuolin antibody 221-1-1 to stain late endosomes (Rauchenberger *et al.*, 1997), and a polyclonal GFP antibody (Clontech). Primary antibodies were diluted 1:5 before use or 1:200 in the case of the polyclonal GFP antibody. After washing with PBS and PBS/3% BSA, cells were incubated for 20 min in Cy3-labeled secondary antibody (Amersham Buchler) diluted 1:500. Nuclei were stained with 0.1 μg/ml 4′,6′-diamidino-2-phenylindole (DAPI) for 5 min. Coverslips were mounted on glass slides with Moviol (Heimer and Taylor, 1974). Double immunofluorescence was performed using Cy3-labeled secondary antibodies together with Alexa488-labeled secondary antibodies (Molecular Probes, Leiden, Germany). Images were recorded on a Zeiss Axiovert 135 inverted microscope equipped with a Quantix camera (Photometrics, Tucson, AZ), controlled by IP-Lab software. For confocal microscopy, a confocal microscope DM/IRB (Leica, Nussloch, Germany) was used, and optical sections were recorded at 0.4 μm per vertical step and 8 times averaging.

Video Microscopy

For video microscopy, cells were transferred to covered chamber glasses (Nunc, Naperville, IN). Sequences were recorded in real time on videotape using a Sony SSC-370CE video camera with an Argus 20 controller (Hamamatsu Photonics, Herrsching, Germany). Time lapse series were acquired using the Photometrics Quantix camera and transferred to a Macintosh 9500 for analysis and storage.

Synchronous morphological differentiation was induced by starvation on MMC agar (20 mM 2-(*N*-morpholino)ethanesulfonic acid [MES], pH 6.8; 2 mM $MgCl_2$; 0.2 mM $CaCl_2$; 2% [wt/vol] Bacto agar [Difco, Detroit, MI]). Structures from various stages of development were visualized using an Olympus B061 microscope (Olympus, Lake Success, NY) and the Sony video camera. A Scion VG-5 frame grabber was used for transfer of images to a Macintosh 9500.

Transmission Electron Microscopy (TEM)

TEM for Figure 9 was performed as described by Novak and coworkers (1995). TEM for Figures 10 and 12 was carried out according to Neuhaus *et al.* (1998).

Measurement of Pinocytosis and Phagocytosis

Fluid-phase endocytosis and exocytosis of surface-attached wild-type Ax2, rescue cells, and *dym*A$^-$ cells were quantitatively analyzed using a method adapted from Bacon *et al.* (1994). Cells were grown to confluency on 6-cm Petri dishes or in shaking culture at a density of 4×10^6 cells/ml. To determine fluid-phase uptake, cells were incubated with 1 mg/ml FITC-dextran in growth medium for various lengths of time. For measuring exocytosis, surface-attached cells were incubated with 1 mg/ml FITC-dextran for 2 h, washed twice, and transferred to fresh growth medium. To determine intracellular transit time of fluid phase, cells were incubated with 5 mg/ml FITC-dextran for 10 min, washed twice, and transferred to fresh medium. At the indicated times, cells were washed twice with 200 mM phosphate buffer, pH 6.3, and once with 50 mM phosphate buffer, pH 9.2. Cells were resuspended in 1 ml 50 mM phosphate buffer, pH 9.2, transferred to tubes, and lysed with 0.4% Triton X-100. After centrifugation the fluorescence of the supernatant was measured in an SLM 8000 spectrofluorimeter at excitation and emission wavelengths of 493 and 516 nm, respectively. The data shown were normalized with respect to total protein content of the cells, as determined with Bradford reagent (Bio-Rad).

Phagocytic ability was measured by a modification to the method of Temesvari and co-workers (1996). Briefly, 1-μm carboxylate-modified, fluorescent polystyrene beads (Molecular Probes) were incubated with cells grown in shaking suspension culture to 3×10^6/ml. The ratio of cells to beads was 1:100. Samples (1 ml) were mixed with 4 ml ice-cold MES buffer, pH 6.5, and placed on a 8-ml cushion of 20% PEG 8000 in MES buffer. Centrifugation at $2000 \times g$ for 10 min separated ingested beads from uningested and attached beads. The uppermost layer and the cushion were removed by careful aspiration, and the cell pellet was washed in 5 mM glycine, 100 mM sucrose, pH 8.5. Cells were lysed in 100 μl of the same buffer containing 1% octylglucopyranosid. Samples were diluted to 1 ml, and fluorescence intensities were measured using excitation and emission wavelengths of 595 and 644 nm, respectively. Normalization of data to total protein content was as described above.

Functional Analysis of the Contractile Vacuolar System

To assess the function of the contractile vacuolar system the method described by Kuwayama and colleagues (1996) was used. Amebae were harvested by centrifugation, washed free of medium, and starved for 1 h in phosphate buffer. Cells were incubated in the presence of 300 mM glucose, water, or phosphate buffer as different osmotic environments in plastic tissue culture dishes. Cells were then monitored visually by video microscopy as described above. For quantitative analysis of viability after treatment a certain amount of cells were plated on bacteria lawns and the number of colonies counted after 4 d.

Functional Analysis of the Mitochondrial System

To assess the function of the mitochondrial system, the activity of the mitochondrial marker succinate dehydrogenase was measured in whole-cell lysates as described by Morré and co-workers (1987). As a control, the activity of the cytoplasmic marker alkaline phosphatase was determined. Cells were washed in MES buffer, resuspended at 3×10^7 cells/ml, and lysed by forced passage through a 5-μm pore filter (Schleicher & Schüll). To measure succinate dehydrogenase activity, 10–50 μl of whole-cell lysate were mixed with a buffer containing 40 mM sodium phosphate (pH 7.4), 250 μg/ml tetranitroblue tetrazoliumchloride (Sigma), 10 mM sodium succinate to a final volume of 500 μl and incubated at room temperature. After 30–60 min the reaction was stopped by the addition of 500 μl 4% SDS, and absorbance was measured at 570 nm.

Alkaline phosphatase activity was measured by mixing 10–50 μl of whole cell lysate with a solution consisting of 50 mM Tris-HCl (pH 9.0), 10 mM $MgCl_2$, and 2.6 mg/ml *p*-nitrophenyl phosphatase (Sigma) to a final volume of 1 ml. After incubation for 30 min at room temperature, absorbance was measured at 404 nm. The data obtained in the succinate dehydrogenase assay were normalized for protein content or alkaline phosphatase activity.

RESULTS

We used PCR techniques to identify *dym*A, the gene encoding dynamin A. Both cDNA and gDNA libraries were screened to obtain a full-length *dym*A clone. Comparison of cDNA and gDNA revealed a single 83-bp intron near the 5′- end of the gene.

The nucleotide sequence of *dym*A revealed an open reading frame of 2559 bp encoding the 853-amino acid polypeptide chain of dynamin A (Figure 1A). With a calculated molecular mass of 96.1 kDa, dynamin A is similar in size to other members of the dynamin family (Obar *et al.*, 1990, van der Bliek and Meyerowitz, 1991, Guan *et al.*, 1993). Dynamin A contains the dynamin consensus motif LPRGSGIVTR (residues 51–60) and sequences corresponding to the tripartite GTP-binding motif (Bourne *et al.*, 1991). The high homology of dynamin A to other members of the dynamin family is mainly confined to the N terminus. For the first 360 amino acids the sequence identity is 57% to rat DLP1, 56% to human dynamin-1, 54% to *D. melanogaster* shibire protein, and 55% to yeast Dnm1p (Figure 1B). The GGARI motif (residues 360–364) marks the carboxy-terminal end of the region of high similarity between dynamin A and the shibire-like dynamins. As previously described for all dynamin-like GTPases, the C terminus shows a higher level of sequence divergence. In the central part of dynamin A (residues 365–500), the highest degree of sequence similarity is observed with DLP1 (49%), Dnm1p (43.0%), and Vps1p (38.3%).

The region of dynamin A formed by residues 500–730 shows no similarity to the primary sequence of other members of the dynamin family. Secondary structure analysis shows that this region is highly hydrophilic and has a high surface probability. This part of dynamin A is almost devoid of charged residues, but is rich in polar amino acids (67%) and contains a high proportion of glutamine (25%), asparagine (23%), and serine (14%) residues that appear in long stretches of up to 13 amino acids (Figure 1A). The central part of the QNS-rich region, corresponding to residues 573–624, comes closest to the proline-rich domain observed with other dynamin family members. This region is basic in composition (pI = 10.0), and 12 of 51 residues are prolines.

The C-terminal domain of dynamin A (residues 730–853) shares 51 and 43% sequence identity with the corresponding regions of DPL1 and Dnm1p. This part of the protein is predicted to be α-helical and marked by an abundance of charged residues (40%), with the number of basic residues (20) almost equaling the number of acidic residues (22). The C-terminal end of classical dynamins is formed by a basic, proline- and arginine-rich domain (PRD) that exhibits no significant sequence similarity to that of dynamin A. However, residues 660–742 of dynamin-1 share 43% sequence identity with residues 730–853 of dynamin A (Figure 1C). This 13-kDa domain of dynamin-1 corresponds to a GTPase effector domain (GED) and is required for efficient GTPase activity (Muhlberg *et al.*, 1997).

After lysis of wild-type cells and cells overproducing the protein, dynamin A was predominantly (~90%) found in the soluble fraction (Figure 2). Further subcellular fractionation of the membrane-associated protein by sucrose gradient centrifugation showed the protein to be enriched in the microsomal fraction (data not shown). The polyclonal antibody PAD1, specific for the N-terminal 380 amino acids of dynamin A, was used for immunoblot analysis. This antibody reacts predominantly with a 96-kDa antigen in whole-cell lysates of Ax2 (see below). The size of the detected antigen agrees well with that of the purified protein (Wienke *et al.*, 1997) and the molecular mass of dynamin A deduced from its amino acid sequence.

Generation of dymA$^-$ Cells by Gene Replacement

The *dym*A locus was disrupted by transforming wild-type Ax2 cells with linearized replacement fragments from vector pBS-ΔDYMA, using resistance against blasticidin S as a selectable marker. After 5–8 d of selection, typically 100–150 colonies were obtained. Thirty to 40 transformants were cloned and screened for the disruption of the *dym*A gene by PCR (data not shown). In three independent experiments, screening indicated that 5–15% of the transformants were potentially *dym*A$^-$. The frequency of the desired recombination event was higher (30–40%) when the replacement fragment was gel purified before transformation.

Positive transformants from the PCR screen were analyzed by Southern blotting to confirm the disruption of the *dym*A gene locus and to determine its molecular organization in the mutant strains. A 0.6-kb

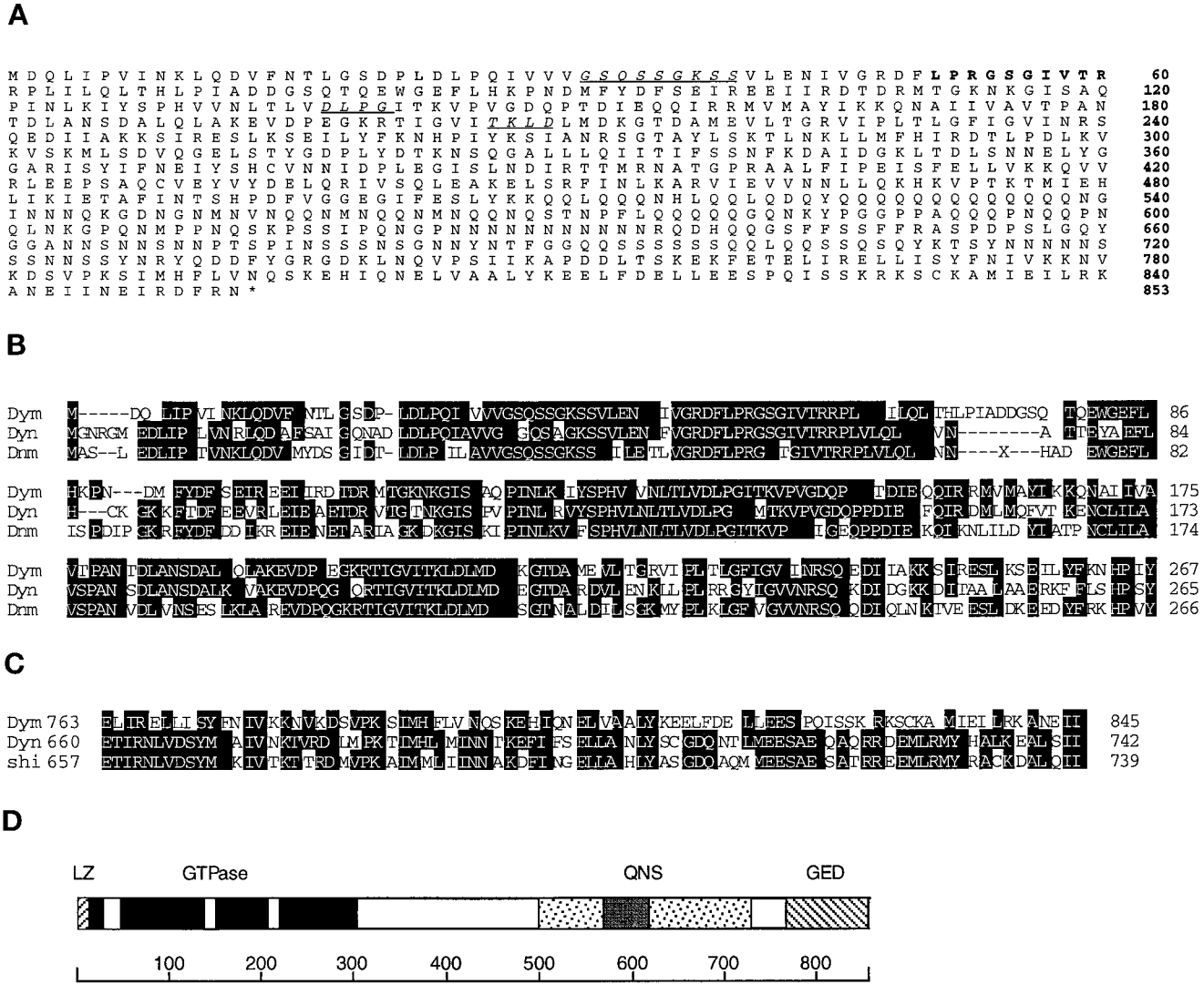

Figure 1. Sequence analysis of *D. discoideum* dynamin A. (A) Predicted amino acid sequence of dynamin A. Dynamin A has a calculated molecular mass of 96.1 kDa and an isoelectric point of 7.0. The tripartite GTP-binding motif is underlined. (B) Sequence alignment of the GTP-binding domains of *D. discoideum* dynamin A (top), human dynamin-1 (middle), and yeast Dnm1p (bottom). An insert in the Dnm1p sequence corresponding to residues 73–114 was omitted from the alignment. The position of the insert is marked by an X in the alignment. Gaps are presented as —. (C) Sequence alignment of the putative GTPase effector domains of dynamin A, human dynamin-1, and the *shibire* gene product. (D) Diagram of dynamin A structural domains. The GTPase domain is shown in solid black, and the tripartite GTP-binding motif is indicated as white bars. LZ, leucine zipper; GED, GTPase effector domain; QNS, glutamine-asparagine-serine-rich domain. The basic, proline-rich part of the QNS-rich region, corresponding to residues 573 to 624, is shown in dark gray.

fragment from the 5′-end of the *dym*A cDNA was used as a probe. The expected hybridization pattern for this probe with wild-type DNA is depicted in Figure 3A. Homologous recombination with the replacement construct is expected to cause a band shift for the *Xba*I–*Eco*RI digest from 7.5 to 3.3 kb and for the *Cla*I digest from 2.6 to 3.8 kb in the *dym*A$^-$ cells (Figure 3B). The Southern blot in Figure 3C is consistent with the predicted change in the hybridization pattern. Further Southern blot analysis with the blasticidin resistance cassette as a probe confirmed that only one copy

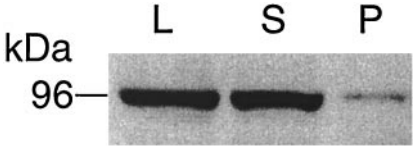

Figure 2. Cellular distribution of dynamin A. Dynamin A is abundant in cytosol. Immunoblots stained with anti-dynamin A antibody PAD1 showing *D. discoideum* whole-cell lysate (L), supernatant after 15 min centrifugation at 15,000 × *g* (S), and pellet (P).

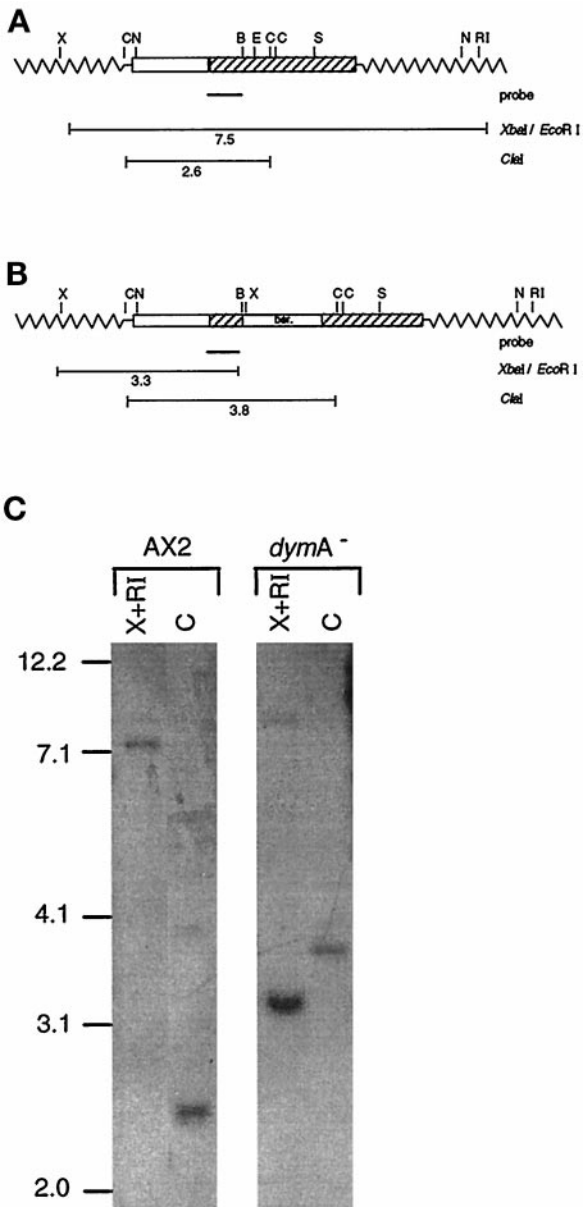

Figure 3. Disruption of *dym*A by gene replacement. (A) Known map of wild-type *dym*A locus. (B) Map of *dym*A$^-$ cells as derived from the Southern blot shown in C. The lighter lines with numbers underneath indicate the size of the restriction fragment (in kilobases) hybridizing with the probe when genomic DNA is digested with the enzymes shown on the right (X, *Xba*I; C, *Cla*I; N, *Nde*I; B, *Bam*HI; E, *Eco*RV; S, *Spe*I; RI, *Eco*RI).

of the replacement fragment had been integrated in the *dym*A gene and no other gene loci had been affected (data not shown). Cell lines HDM1701, HDM1702, and HDM1703, each with a disrupted *dym*A gene locus, were obtained from three different transformations and will be referred to, in the following text, as *dym*A$^-$ cells.

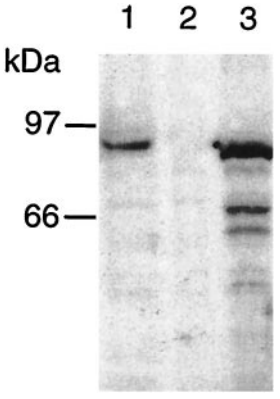

Figure 4. Immunoblot analysis of *dym*A$^-$ cells. Whole-cell protein (50 μg) from Ax2 cells (lane 1), *dym*A$^-$ cells (lane 2), and *dym*A$^-$ cells rescued by transformation with a plasmid bearing the wild-type *dym*A gene (lane 3) were separated on a 12% SDS-PAGE gel, blotted, and probed with polyclonal antibody PAD1 directed against the 380 N-terminal residues of dynamin A.

As expected from the disruption of the *dym*A gene locus, the 96-kDa antigen was not detectable in whole-cell lysates of *dym*A$^-$ cells by immunoblot analysis (Figure 4, lane 2).

Complementation of the dymA$^-$ Cells

To confirm that phenotypic changes in the *dym*A$^-$ cells are explicitly attributable to the loss of the *dym*A gene product, the mutant strain was rescued by reintroduction of functional copies of *dym*A. The multicopy plasmid pDX-DYMA, harboring the entire *dym*A gene under the control of its native promoter, was used to transform *dym*A$^-$ cells. Complementation of *dym*A$^-$ cells led to the production of the 96-kDa antigen at levels 10- to 50-fold higher than those observed for Ax2 cells (Figure 4, lane 3) and rescued all phenotypic changes observed with dynamin A-depleted cells.

Growth and Appearance of dymA$^-$Cells

The *dym*A gene product is not essential for *D. discoideum* growth. However, *dym*A$^-$ cells grow under all conditions tested approximately twofold slower than the parental Ax2 cells. In axenic media, Ax2 cells grow with doubling times <12 h. Exponentially growing cultures of *dym*A$^-$ cells double every 24 h under the same conditions. In suspension culture, Ax2 cells reach cell densities of 1×10^7 cells/ml and above while *dym*A$^-$ cells grow to a maximum cell density of 2×10^6 cells/ml.

Unusually large cells and the frequent occurrence of cytoplasmic bridges connecting neighboring cells are prominent features of populations of surface-attached *dym*A$^-$ cells (Figure 5A). Staining with DAPI showed that most *dym*A$^-$ cells are multinucleated with 40% of

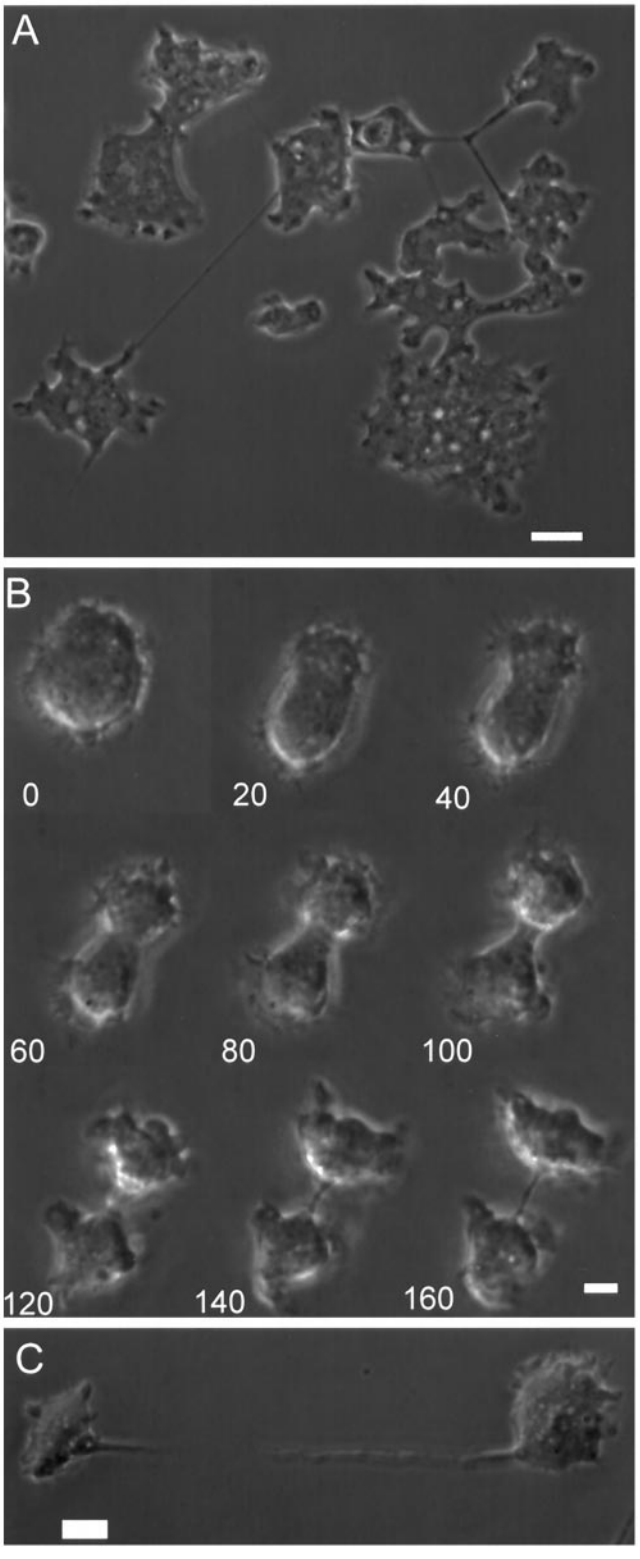

Figure 5. Cell division in *dym*A$^-$ cells. (A) Populations of dynamin A-deficient cells contain many unusually large cells, some of which are connected via cytoplasmic bridges. After transfer from suspension culture to a Petri dish or a similar substratum *dym*A$^-$, cells frequently divide by amitotic traction-mediated cytofission. (B) Time-lapse video microscopy demonstrated that *dym*A$^-$ cells are able to pass through all the phases of cell division at wild-type speed. The defect only occurs at the final stage of cytokinesis, at which the incipient daughter cells are merely connected by a cytoplasmic bridge. Images were taken at 20-s intervals. (C) In wild-type cells this connection was usually short lived, while the long cytoplasmic bridges of *dym*A$^-$ cells persisted for several minutes to several hours and reached more than 100 μm in length. Bar, 10 μm.

the cells containing three or more nuclei and some upwards of 20 nuclei. This is in comparison to wild-type cells where 98% of the cells have one or two nuclei with <2% having three or more nuclei. The frequent occurrence of large multinucleated cells and cytoplasmic bridges is reminiscent of myosin II-defective cells, which are unable to carry out normal cytokinesis and whose ability to divide requires attachment to a surface (De Lozanne and Spudich, 1987; Neujahr *et al.*, 1997).

However, unlike myosin II-depleted cells, *dym*A$^-$ cells are able to grow in suspension culture. When *dym*A$^-$ cells are transferred from shaken culture to Petri dishes, the multinucleated cells start within minutes to undergo amitotic cell divisions by tearing themselves into smaller fragments by traction-mediated cytoplasmic fission (Figure 5A). Amitotic cell divisions are also observed at an increased frequency shortly after the transfer of *dym*A$^-$ cells to nutrient-free salt solutions. However, when cells are grown axenically or in association with bacteria, cytokinesis is in most instances (<95%) synchronized with mitosis. We used time-lapse video microscopy to follow cytokinesis in surface-attached and synchronized *dym*A$^-$ and Ax2 cells. The timing and the sequence of shape changes during cytokinesis were similar for both strains. Approximately 2–3 min were required to pass through cleavage furrow constriction until only a thin filamentous connection persisted (Figure 5B). This connection is very short lived in wild-type cells. In all recorded events the connection broke within 2 min and reached a maximal length of 20 μm. In contrast, long cytoplasmic bridges are a distinct phenotypic feature of surface-attached *dym*A$^-$ cells (Figure 5C). They persist for several minutes to several hours and reach up to 300 μm in length. The incipient daughter cells can undergo additional rounds of cytokinesis without disruption of the cytoplasmic bridges, leading to networks of interconnected cells. As long as the cytoplasmic bridges persist, the almost completely separated daughter cells can fuse again, thus giving rise to large multinucleated cells. A similar defect in cytokinesis was previously reported for calmodulin-depleted *D. discoideum* cells (Liu *et al.*, 1992).

The average *dym*A$^-$ cell appears to lack polarity but is highly dynamic (Figure 6). Cells were frequently observed to cyclically extend and retract lamellopodia

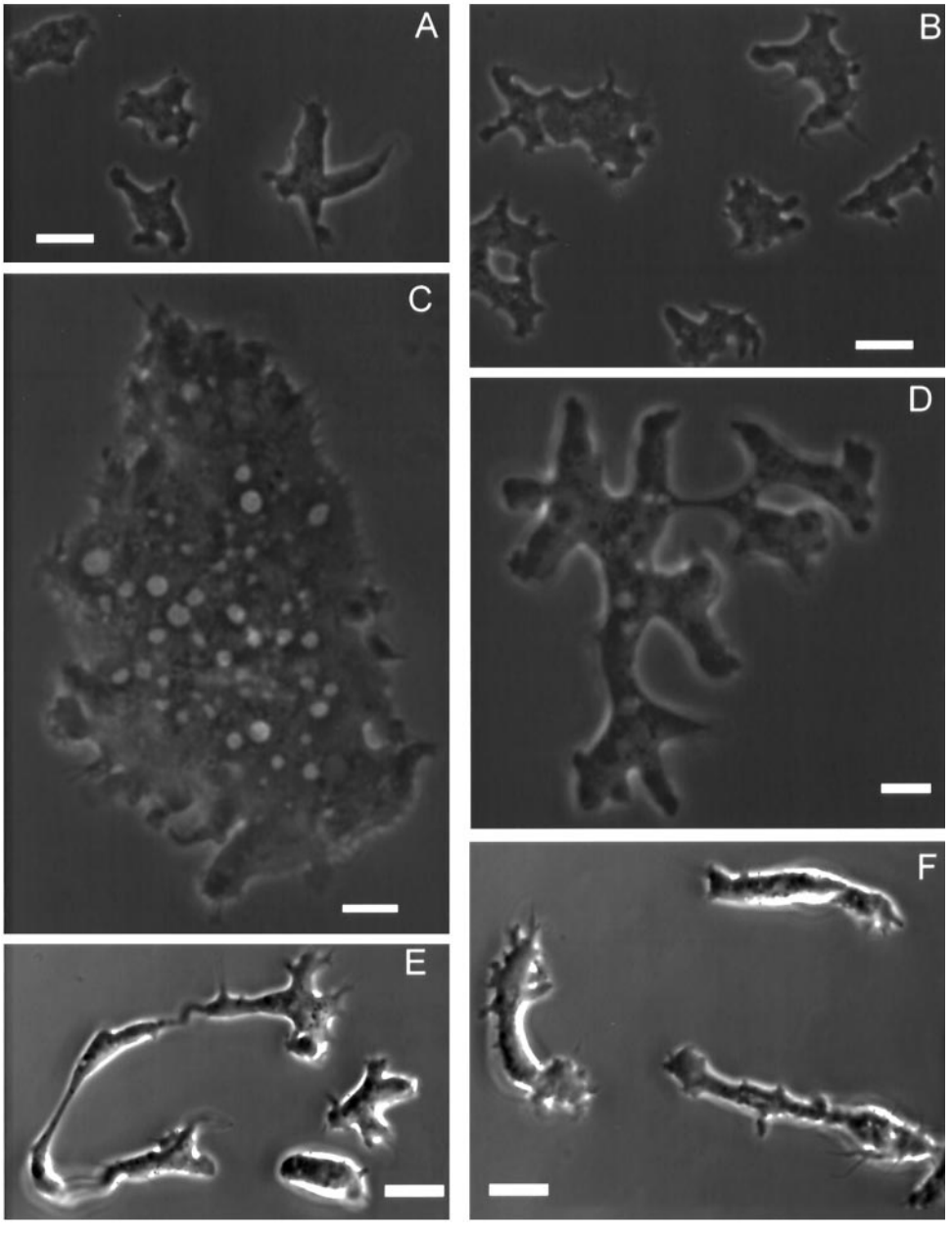

Figure 6. Cells lacking dynamin A are large and irregularly shaped and show multiple pseudopodia. (A) Phase-contrast micrograph of untransformed Ax2 cells in axenic culture. (B) Phase-contrast micrograph of Ax2 cells 4 h after transfer in a nutrient-free, buffered salt solution. (C and D) Dynamin A-depleted cells show a striking difference in size and morphology and appear apolar in axenic culture. (E and F) When placed under starvation conditions for 4 to 5 h, *dym*A$^-$ cells take on a very elongated shape, form many cell surface projections, and show increased motile activity. Bar, 10 μm.

around the entire cell periphery. Pseudopodial extensions and long filopodia were also commonly observed; however, their distribution on the cell surface appears random. When we measured the speed of cells undergoing random walks on a glass surface, we found that *dym*A$^-$ cells are very motile and move at rates similar or greater than those observed for wild-type cells. Cell movement was measured under two different nutrient conditions. First, in axenic medium, *dym*A$^-$ cells moved at a rate of 4.4 μm/min (SD $\pm$ 2.7; n = 98) and Ax2 cells at 4.7 μm/min (SD $\pm$ 2.9; n = 86). Second, movement was tested after transfer to a buffered salt solution. The motility of *D. discoideum* cells varies with the developmental stage and reaches

a maximum at the onset of aggregation about 8 h after transfer to starvation conditions (Varnum *et al*., 1985). Thus, transfer to starvation conditions induced an increase in the velocity of Ax2 cells to 5.8 μm/min (SD ± 3.2; n = 74) compared with vegetative cells. The maximum velocity of *dym*A$^-$ cells was 6.8 μm/min (SD ± 3.2; n = 74) during early development. Simultaneously, the multinucleated *dym*A$^-$ cells undergo several rounds of traction-mediated cytoplasmic fission, which inhibits the directed movement of the cells. The chemotactic response of *dym*A$^-$cells was normal (data not shown).

Development

The developmental program of *D. discoideum* is initiated upon starvation. Cells start emitting cAMP pulses and aggregate into mounds consisting of ~10^5 cells. These mounds undergo a series of morphological changes that culminate in the formation of a fruiting body (Raper, 1935). The transcriptional regulation of *dym*A expression during development was assessed by probing Northern blots of RNA isolated at a series of developmental stages. A ~3-kb *dym*A transcript was detected in vegetative cells and, at similar levels, at all later developmental stages (data not shown).

When *dym*A$^-$ cells were placed in starvation conditions on nonnutrient agar plates, the cells took 10 h to start streaming in comparison to 7 h observed for wild-type cells. Except for this difference in timing, early development of *dym*A$^-$ cells appeared similar to that of the wild-type cells. The delay in the onset of streaming of *dym*A$^-$ cells may, in part, be explained by the requirement to undergo several rounds of cytokinesis by traction mediated cytofission before efficient development can be initiated. Development of *dym*A$^-$ cells is completed by 30–36 h, while Ax2 cells completed development within 24–26 h. The final developmental morphology of *dym*A$^-$ cells results in shorter fruiting bodies consisting of a tapered stalk with enlarged basal disk and spore mass at the apical tip and a second cluster of spores laterally attached to the center of the stalk (Figure 7B). Only 10–20% of the spores formed by *dym*A$^-$ cells were resistant to heat treatment and germinated after incubation at 42°C for 30 min, in contrast to ~90% for wild-type cells (data not shown).

When *D. discoideum* cells are plated at low density in association with bacteria on nutrient agar plates, the bacteria form a confluent lawn and the *D. discoideum* cells form clonal plaques within the lawn as the bacteria are digested. Consistent with their reduced rate of growth under axenic conditions, the rate at which *dym*A$^-$ cells advanced on a bacterial lawn was approximately twofold slower than that of wild-type cells. In areas behind the advancing edge, where the *dym*A$^-$ cells had depleted the bacteria, the cells starved and gave rise to fruiting bodies that resembled those observed on nonnutrient agar plates.

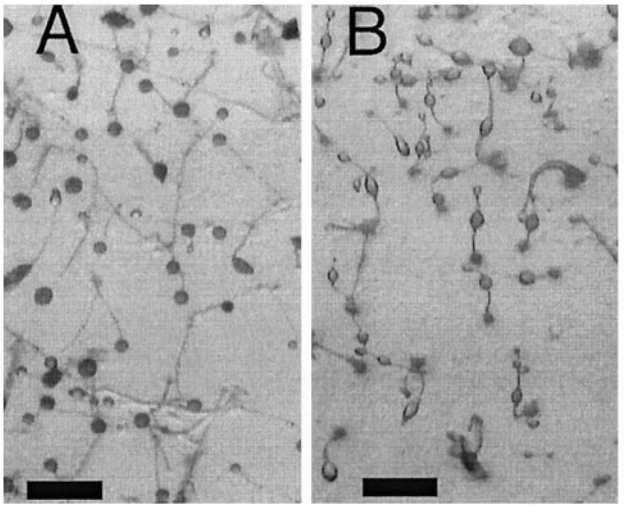

Figure 7. Development of fruiting bodies in wild-type Ax2 and *dym*A$^-$ cells. In comparison to the Ax2 cells (A) the final developmental morphology of *dym*A$^-$ cells results in shorter fruiting bodies consisting of a tapered stalk with enlarged basal disk and spore mass at the apical tip and a second cluster of spores laterally attached to the center of the stalk (B). Bar, 1 mm.

Endocytosis and Osmoregulation in dymA$^-$ Cells

The role of dynamin A in the endosomal-lysosomal system of *D. discoideum* was tested by measuring the uptake of the fluid phase marker fluorescein-labeled dextran. In comparison to cells containing a functional copy of *dym*A, the extent to which the marker was accumulated was approximately twofold reduced in *dym*A$^-$ cells (Figure 8A). The initial rate of uptake for the first 40 min was 33% slower for *dym*A$^-$ than the parental wild-type or rescue cells. Thus, the lack of a dynamin A has a clear inhibitory effect on the initial rate of internalization and the long-term accumulation of the fluid phase marker. Similar results were obtained for cells grown on a substratum or in suspension.

The release of fluid phase marker over time was measured to show that the reduced rate of FITC-dextran uptake by the *dym*A$^-$ cells can be attributed to a deficiency in internalization and not recycling to the media by a faster rate of exocytosis. Cells were loaded for 2 h with FITC-dextran, washed free of the marker, and resuspended in fresh medium. The amount of fluid-phase marker that remained in the cells over time was measured. Similar rates of exocytosis were determined for *dym*A$^-$ cells and cells producing dynamin A (Figure 8B).

Examination of intracellular transit time by exposing the cells to a 10-min pulse of FITC-dextran re-

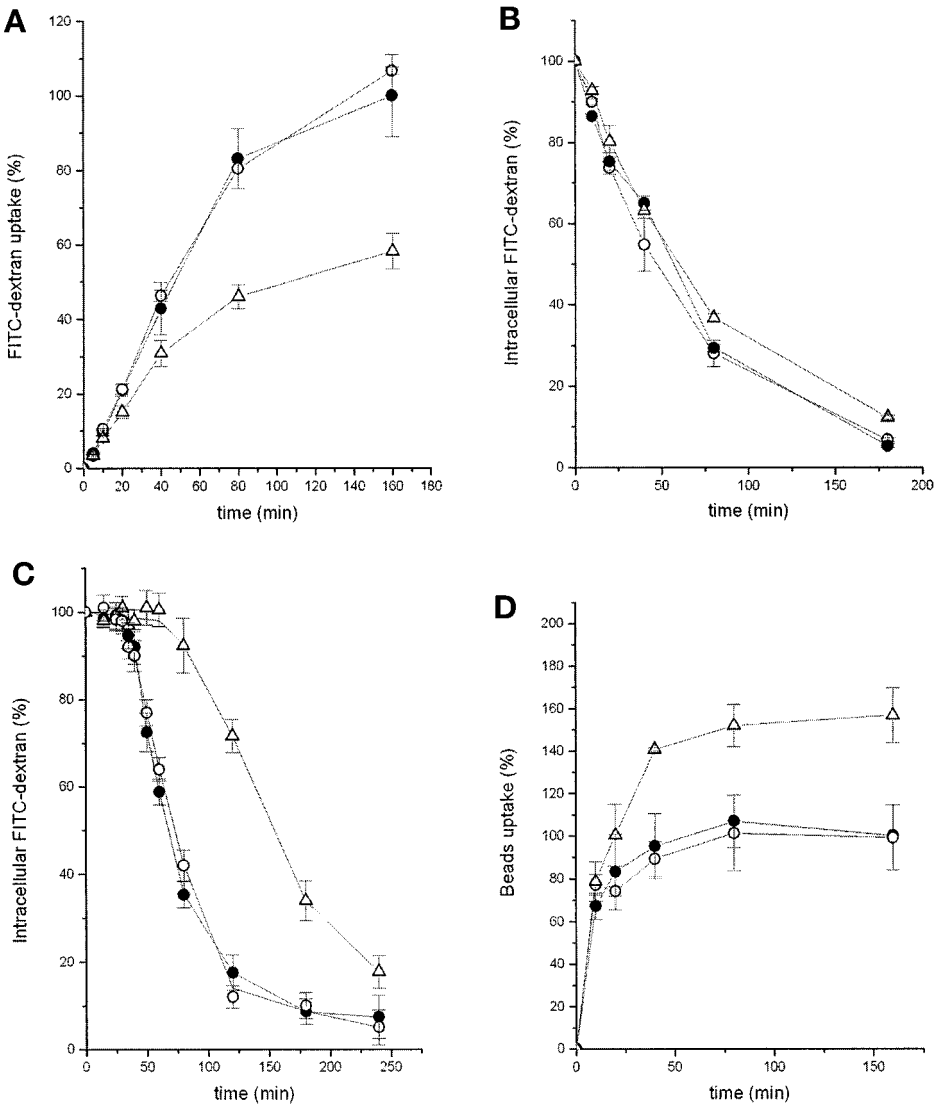

Figure 8. The role of dynamin A in pinocytosis and phagocytosis. For quantification of fluid-phase marker uptake, cells were incubated with 1 mg/ml FITC-dextran, and intracellular fluorescence was measured at the time points indicated. The amount of FITC-dextran internalized was plotted as percent of total uptake of Ax2 cells after 160 min. (A) In comparison to wild-type Ax2 cells (closed circles) and a rescued cell line (open circles), the extent to which the marker was accumulated was approximately twofold reduced in *dym*A$^-$ cells (open triangles). The initial rate of uptake for the first 40 min was 33% slower for *dym*A$^-$ than the parental wild-type or rescue cells. (B) For analysis of exocytosis, cells were incubated with 1 mg/ml FITC-dextran for 2 h, washed, and incubated with fresh medium for the time points indicated. Intracellular fluorescence was measured and plotted as percent of FITC-dextran remaining in the cells. Similar rates of exocytosis were determined for *dym*A$^-$ cells and cells producing dynamin A. (C) Intracellular transit time of fluid phase was measured by incubating the cells in 5 mg/ml FITC-dextran for 10 min and transfer to fresh media for the time indicated. Intracellular fluorescence was measured and plotted as percent of FITC-dextran remaining in the cells. In *dym*A$^-$ cells transit time was prolonged more than twofold. (D) Phagocytotic ability was assayed by following the uptake of 1 μm polystyrene microspheres (100 beads/cell) in axenic medium. In *dym*A$^-$ cells phagocytosis is increased by 50% compared with control cells. All the assay data are normalized to protein content and represent averages from at least three independent experiments.

vealed that the retention of the marker is more than twofold prolonged in *dym*A$^-$ compared with wild-type and rescue cells. The half-life for internalized FITC-dextran was 60 min in control cells and 150 min in *dym*A$^-$ cells (Figure 8C).

Phagocytosis is an inducible actin-dependent process. It is initiated by adhesion of a particle to any region on the surface of a *D. discoideum* cell. To investigate whether dynamin A plays a role in phagocytosis, *dym*A$^-$ and control cells were incubated with fluorescent polystyrene beads of 1 μm diameter for various lengths of time. In contrast to the pinocytosis assays, particle uptake experiments were performed with cells grown in shaking suspension culture. Compared with Ax2 and rescue cells, the *dym*A$^-$ mutants exhibited a 50% increase of total particle uptake (Figure 8D).

The best characterized function of dynamin-1 is its role in receptor-mediated endocytosis via clathrin-coated pits (Herskovits *et al.*, 1993; van der Bliek *et al.*, 1993; Takei *et al.*, 1995). Therefore, we were particularly interested in comparing the phenotype of *dym*A$^-$ cells and clathrin heavy chain-deficient *D. discoideum* cells (CHC$^-$ cells). Coated vesicles are particularly enriched near the microtubule-organizing center (MTOC) of wild-type cells and were found to be completely absent in CHC$^-$ cells (O'Halloran and Anderson, 1992). In *dym*A$^-$ cells, coated vesicles were observed throughout the cytoplasm and in large numbers (>20) near the MTOC. Coated pits were frequently observed in association with larger vesicles but not at the plasma membrane. One of the most prominent defects of CHC$^-$ cells is the absence of large vacuoles that form part of the contractile vacuole

system (Ruscetti *et al.*, 1994). Examination of the morphology and function of this osmoregulatory organelle in *dym*A$^-$ cells showed the contractile vacuole system to function normally. Observation of *dym*A$^-$ cells by phase microscopy revealed the cyclic filling and emptying of large vacuoles. Exposure to hypo- and hyperosmotic conditions had no adverse effect on the viability of *dym*A$^-$ cells. Localization of two contractile vacuole markers, calmodulin and the 100-kDa subunit of the V-H$^+$-ATPase (Fok *et al.*, 1993; Zhu *et al.*, 1993), by immunofluorescence revealed no difference in the appearance and organization of the contractile vacuole system of *dym*A$^-$ cells and that of the parental cell line (data not shown).

Disruption of dymA Affects Organelle Morphology

The clear differences in cell morphology between Ax2 cells and *dym*A$^-$ cells led us to examine the ultrastructure of *dym*A$^-$ cells at light and electron microscopic levels. Transmission electron micrographs showed a striking accumulation of membrane tubules in proximity to nuclei and the cell membrane in *dym*A$^-$ cells (Figures 9 and 10). These spongiome-like structures could represent sections through convoluted vesicular or tubular profiles. Additionally, coated vesicles (90–150 nm) or pits could be readily detected in electron microscopic (EM) micrographs of *dym*A$^-$ cells, and the number of coated structures appeared higher than in wild-type cells. Coated vesicles were observed in association with spongiome-like structures and were particularly enriched near the MTOC (Figure 10, A and B). Coated pits were frequently found on vesicular or tubular structures near the plasma membrane but not at the plasma membrane itself (Figure 10, C and D).

The localization of proteins related to the endolysosomal system and the Golgi complex was investigated by immunofluorescence, to identify the nature of the spongiome-like compartment (Figure 11). No differences were observed for endosomal compartments that can be detected with an antibody that recognizes the actin-binding protein coronin (De Hostos *et al.*, 1991). However, when anti-vacuolin antibody 221-1-1 was used for staining late endosomal compartments (Rauchenberger *et al.*, 1997), the immunofluorescence pattern in *dym*A$^-$ cells was clearly altered. Two to four late endosomes of similar size were observed per nucleus in Ax2 cells. In contrast, the number of stained vesicles per nucleus is increased to 10 or more in *dym*A$^-$ cells. The vacuolin-positive compartment of *dym*A$^-$ cells is more variable in size and seems to form a tubular network compared with the discrete ring-like structures observed in Ax2 cells (Figure 11, A and A′). Cellular localization of GFP–dynamin A by immunofluorescence microscopy produced a similar, but more punctate, labeling of

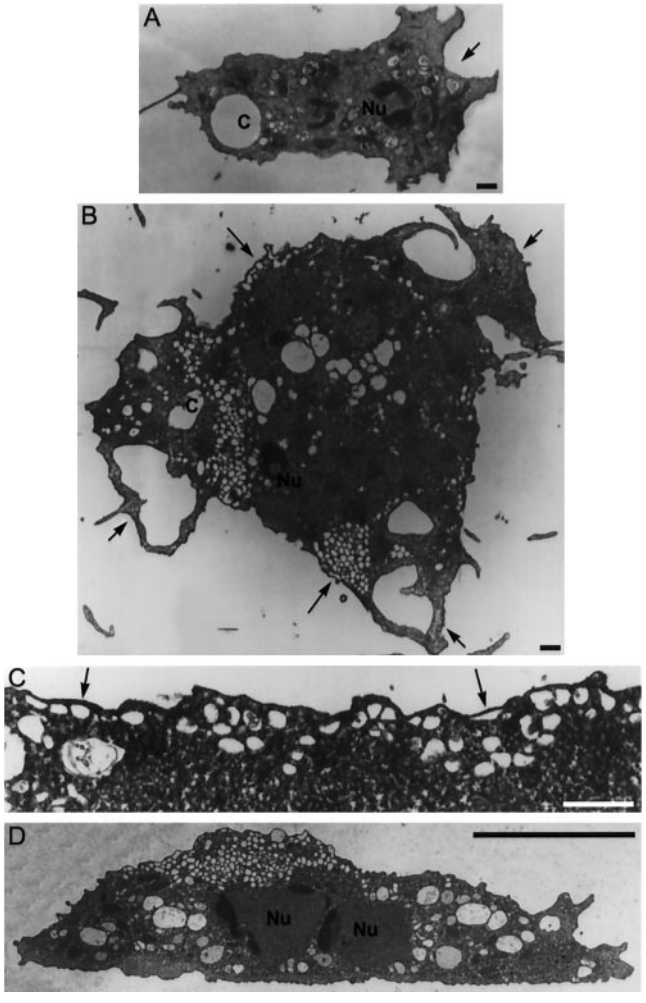

Figure 9. Representative electron micrographs of wild-type and *dym*A$^-$ cells. Panels A, B, and C represent sections parallel to the surface of attachment. (D) This panel represents a perpendicular section. (A) Wild-type cells are smaller, with single nuclei (Nu) and one or two contractile vacuoles (c) with a few associated small vesicular or tubular profiles. Wild-type cells show a single main extension (arrow), reflecting movement in a particular direction. (B–D) Most *dym*A$^-$ cells are very large. However, due to limitations on illustration size, panels B and D show smaller *dym*A$^-$ cells that nevertheless illustrate the most important features of the *dym*A$^-$ phenotype. In contrast to wild-type cells, *dym*A$^-$ cells extend processes in several directions (short arrows) and display areas with numerous small vesicular profiles (long arrows) that may be sections through discrete vesicles or convoluted tubules. (C) Higher magnification of a region (arrows) showing many vesicular profiles under the cell membrane. Magnification in panels A and B is the same. Bar, 1 μm in panels A–C and 10 μm in panel D.

membranous structures, and double immunofluorescence showed an almost complete colocalization of vacuolin and dynamin A (Figure 11B). The organization of the Golgi apparatus was visualized using antibody 190-340-8 (Weiner *et al.*, 1993). Perinuclear structures with short tubular extensions were ob-

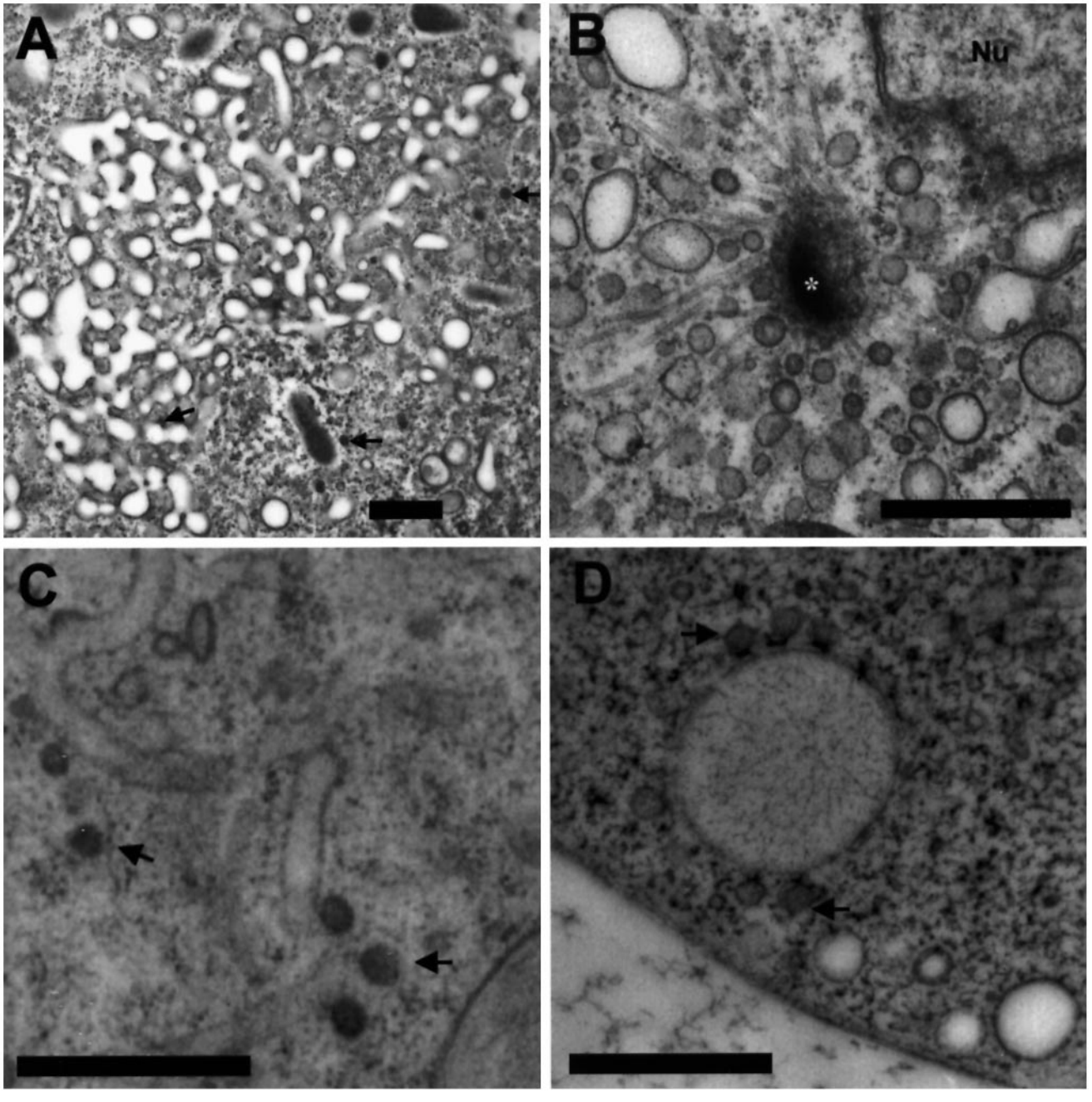

Figure 10. Electron micrographs showing the distribution of coated structures (arrows) in dynamin A-depleted cells. (A) Area with numerous small vesicular profiles that may be sections through discrete vesicles or convoluted tubules. (B) Vesicles and coated vesicles are particularly enriched in the region near the MTOC (asterisk). Part of the cell nucleus (Nu) can be seen in the upper right corner of the panel. (C) Coated structures can be observed throughout the cell in association with tubular membrane structures. (D) Large, coated-pit–decorated vesicles are frequently found near the plasma membrane. Bar, 1 μm.

served in Ax2 (Figure 11C). The perinuclear Golgi network appeared somewhat enlarged in the *dym*A$^-$ cells, and there was a higher background of diffuse staining throughout the cells. The increase in diffuse background staining was also observed in mononucleate *dym*A$^-$ cells of comparable size to the wild-type cells. In larger, multinucleated *dym*A$^-$ cells the prominent juxtanuclear labeling of all nuclei indicated that each was associated with a Golgi complex (data not shown).

The effects of *dym*A disruption were not restricted to the endo-lysosomal system. Normally mitochondria are dispersed uniformly throughout the cytoplasm of *D. discoideum* cells. In *dym*A$^-$ cells, mitochondria form continuous reticular structures of variable diameter that consist primarily of tubules and are branched at multiple points (Figure 12). The striking difference in mitochondrial morphology was best visualized by indirect immunofluorescence (Figure 12, A and A′) using an anti-porin antibody (Troll *et al.*, 1992). Clusters of mitochondria and mitochondria forming continuous reticular structures could also be readily observed in living *dym*A$^-$ cells by phase contrast microscopy or after appropriate fixation by electron microscopy (Figure 12, D–F). In addition to these morphological changes, loss of dynamin A expression appears to affect mitochondrial function. The activity of the respiratory chain-marker enzyme, succinate dehydrogenase, was approximately twofold reduced (47 ± 8%) in homogenates of *dym*A$^-$ cells when compared with wild-type cells.

The EM micrographs also indicated differences in the size and shape of cell nuclei between *dym*A$^-$ cells and the parental Ax2 cells. Cells were stained with the DNA-specific dye DAPI to further investigate these differences in nuclear morphology (Figure 12, B, B′, C, and C′). On average, the nuclear diameters determined for *dym*A$^-$ cells (3.4 ± 0.8 μm; n = 376) and Ax2 cells (3.3 ± 0.5 μm; n = 212) were similar. However, ~2% of *dym*A$^-$ nuclei measured 6–8 μm in diameter while none of the Ax2 nuclei was larger than 6 μm, and only one was larger than 5 μm. In addition to the occurrence of large nuclei in populations of dynamin A-depleted cells, DAPI-stained *dym*A$^-$ nuclei can easily be distinguished from wild-type nuclei by their lobed appearance, indicative of a difference in chromatin organization, and aberrant shape.

DISCUSSION

Dynamin A represents a new member of the family of dynamin-related proteins. The results presented here establish that this *D. discoideum* protein shares hallmark features, such as the tripartite GTP-binding motif, the consensus pattern LPRGSGIVTR, and a high degree of sequence identity with the N-terminal half of other dynamin-like proteins (Figure 1). The C-terminal half of dynamin A contains sequence motifs that could potentially serve roles similar to those of the PRD and GED of dynamin-1. However, the organization of these regions in the polypeptide chain of dynamin A differs from that of dynamin-1. Dynamin A contains a QNS-rich domain, and similar asparagine and glutamine repeats have been found in several other *D. discoideum* proteins, e.g., protein tyrosine phosphatase PTP3 (Gamper *et al.*, 1996) and the catalytic subunit of cAMP-dependent protein kinase PKAC (Burki *et al.*, 1991; Mann and Firtel, 1991). The significance of these repeats is not well understood, but it has been speculated that glutamine repeats may form polar zippers that make protein oligomerize or able to interact with other proteins containing glutamine repeats (Stott *et al.*, 1995). Huntington's disease and six other neurodegenerative diseases have been linked to abnormally expanded stretches of polyglutamine in the affected proteins.

Phylogenetic analysis places dynamin A in the same branch as the yeast proteins, Vps1p and Dnm1p, and the mammalian proteins, DVLP and DLP1. In primary structure and domain organization, dynamin A is more closely related to DLP1 and Dnm1p than dynamin-1. So far, little is known about the biochemical and structural features of this group of dynamin-like proteins. The members of this group of dynamin-like proteins appear to support vesicle trafficking processes at cytoplasmic sites distinct from the plasma membrane. Vps1p is associated with the Golgi and is required for proper sorting of proteins to the yeast vacuole (Vater *et al.*, 1992; Wilsbach and Payne, 1993; Nothwehr *et al.*, 1995). Dnm1p is mostly cytosolic and believed to function primarily in the maintenance of yeast mitochondrial network morphology (Shaw *et al.*, 1997). Human DVLP is predominantly found in the perinuclear region, but its precise role and membrane localization are unknown (Shin *et al.*, 1997). Rat DLP1 is predominately found in the soluble cytosolic fraction, but a substantial amount associates with endoplasmic reticulum tubules and vesicles that move unidirectionally from the cell periphery toward the perinuclear region; it may function in the transport of peripheral endoplasmic reticulum elements to the Golgi compartment (Yoon *et al.*, 1998).

To gain insight into the cellular function of dynamin A, we used gene replacement techniques to create *D. discoideum* cells that no longer produce the protein. The resulting *dym*A$^-$ cells were viable under all conditions tested, indicating that the *dym*A gene product is not essential for *D. discoideum* growth. However, dynamin A-deficient cells displayed pleiotropic phenotypic changes in comparison to the parental Ax2 wild-type cells.

In agreement with a role of dynamin A in vesicle sorting and trafficking, the ability to internalize fluid phase markers by pinocytosis was reduced in *dym*A$^-$ cells. Both the initial rate of uptake and the extent to which the marker was accumulated were affected. At the same time efflux of the fluid phase marker was normal, indicating dynamin A participates in endosomal trafficking, but not in recycling of internalized fluid. The prolonged transit time for fluid phase in the *dym*A$^-$ cells indicates that the intracellular processing of fluid phase cargo is altered. Immunofluorescence analysis was used to further dissect the defect in endocytosis. Coronin, a cytoplasmic actin-associated

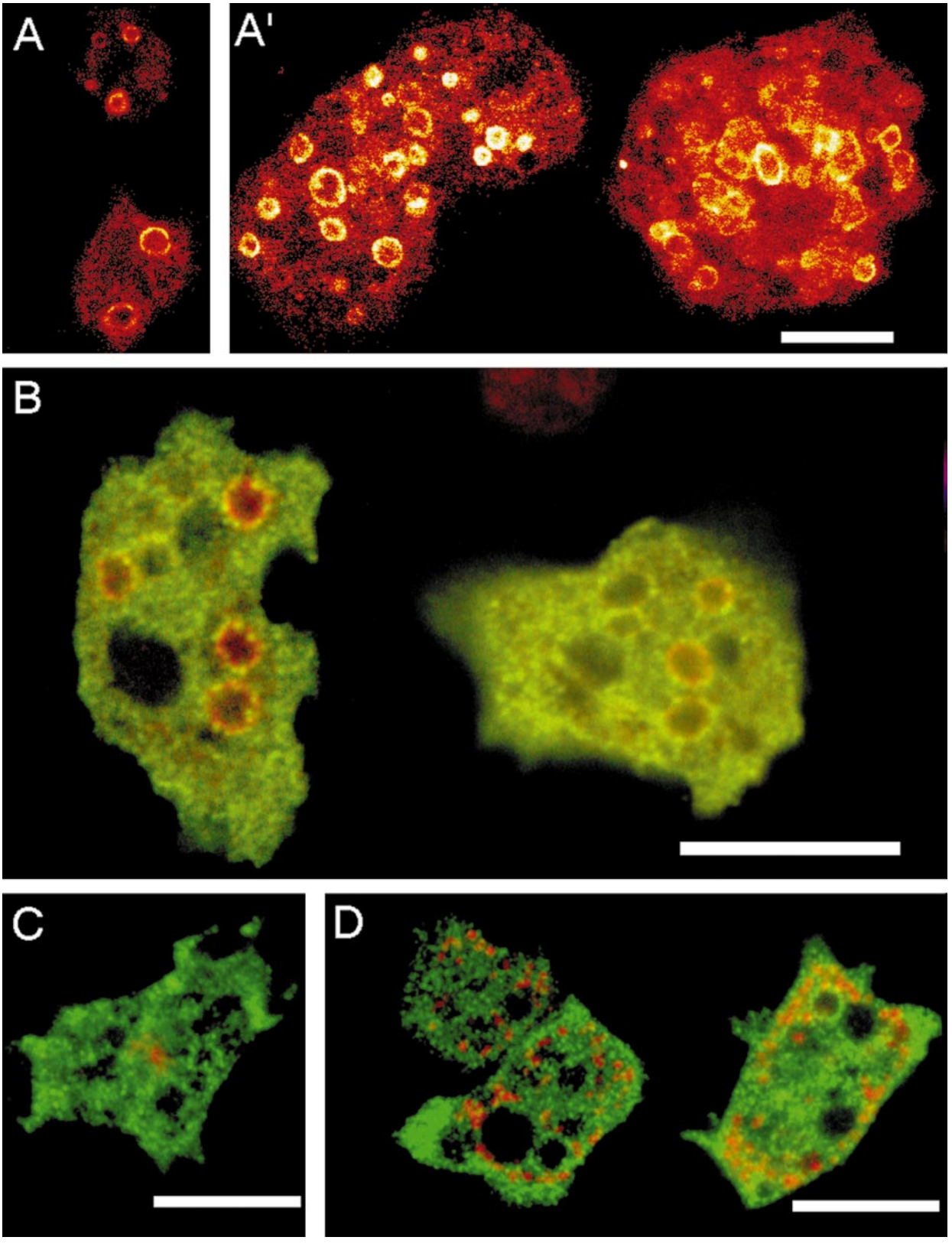

Figure 11.

protein and a marker of endocytic compartments, is strongly enriched in a cytoskeletal coat that transiently surrounds both particle- and fluid-containing vacuoles in *D. discoideum* (Maniak *et al.*, 1995; Hacker *et al.*, 1997). Within the first minute after internalization, both coronin and actin are gradually released from the phagosome or macropinosome. After dissociation of the cytoskeletal coat, acidification and digestion of the vesicle contents occur. The rapid acidification to pH 5 is followed by neutralization and reassociation with a cytoskeletal coat. The ingested cargo is thus progressively shuttled to a large, neutral compartment that acquires fluid-phase markers 60–80 min after endocytosis, just before exocytosis (Rauchenberger *et al.*, 1997). While the cellular localization of coronin and the frequency of coronin-associated vacuolar structures appeared unchanged, the vacuolin-decorated, postlysosomal compartment was greatly enriched in dynamin A-depleted cells and may, at least in part, account for the accumulation of large vacuoles (>300 nm) and tubular structure in these cells (Figures 9 and 10). The colocalization of dynamin A and vacuolin supports the idea that dynamin A might be required for the breakdown of the vacuolin-decorated postlysosomal vesicles.

The role of mammalian dynamin-1 in clathrin-mediated endocytosis is well established (Herskovits *et al.*, 1993; van der Bliek *et al.*, 1993; Damke *et al.*, 1994). It was shown that fluid-phase uptake is affected in a HeLa cell line expressing a temperature-sensitive dynamin mutant. However, after shift to the nonpermissive temperature, these HeLa cells rapidly and completely compensate for the loss of clathrin-dependent endocytosis by inducing an alternate endocytic pathway (Damke *et al.*, 1995; Lamaze and Schmid, 1995). In contrast, pinocytosis is constitutively impaired in *D. discoideum* cells lacking either dynamin A or the clathrin heavy chain (O'Halloran and Anderson, 1992; Ruscetti *et al.*, 1994). Apart from this reduced activity in pinocytosis, the *dym*A$^-$ and CHC$^-$ mutants display a spectrum of common and separate defects. CHC$^-$ and *dym*A$^-$ cells share a defect in cytokinesis. However, while CHC$^-$ cells are unable to grow in suspension cultures and fail to divide due to an inability to form a functional contractile ring during cell division (Niswonger and O'Halloran, 1997a), *dym*A$^-$ cells grow in suspension culture and pass through all stages of cytokinesis up to the formation of the midbody. Only the final step, severing of the thin cytoplasmic bridge connecting the incipient daughter cells, is inhibited in *dym*A$^-$ cells. A distinct defect of the CHC$^-$ cells is the lack of a contractile vacuole and the resulting impairment in osmoregulation. In contrast, the contractile vacuole system of *dym*A$^-$ cells was found to be fully functional, and its morphological organization was similar to that of wild-type cells. The developmental program is affected both in CHC$^-$ and *dym*A$^-$ cells. It was demonstrated that clathrin increases the efficiency of early development and is essential for differentiation of mature spore cells (Niswonger and O'Halloran, 1997b). Dynamin A-deficient cells show a comparable defect in the early stages of development; however, progress from the formation of a pseudoplasmodium to the culmination of the fruiting body was normal. Fruiting bodies formed by dynamin A-deficient cells display significant morphological alterations, but they are still capable of producing viable spores, although spore viability is reduced to 10–20% of wild-type levels. Finally, while CHC$^-$ cells display defects in sorting and secretion of lysosomal enzymes (Ruscetti *et al.*, 1994), this pathway does not seem to be affected by disruption of *dym*A. Lysosomal α-mannosidase is processed normally and apparently not missorted in *dym*A$^-$ cells, and secretion of mature forms of the enzyme also appears to be normal (data not shown).

The strong impairment in endocytosis of fluid phase markers in CHC$^-$ mutants suggested initially that fluid entry proceeds in *D. discoideum* mainly through clathrin-mediated endocytosis (O'Halloran and Anderson, 1992). However, a number of recent studies indicate that, in *D. discoideum*, fluid-phase uptake proceeds predominantly by macropinocytosis and that the reduction in pinocytosis capacity of axenically grown CHC$^-$ cells is caused by cross-talk between the actin- and clathrin-dependent routes of fluid entry during endocytosis (Adessi *et al.*, 1995; Hacker *et al.*, 1997). Similarly, the observed reduction in the uptake of fluid-phase markers by *dym*A$^-$ cells may be an indirect effect of dynamin A depletion. This interpretation is best supported by the observed distribution of coated structures in *dym*A$^-$ cells and is in agreement with a general role of dynamins in the budding

Figure 11 (facing page). Immunolocalization of dynamin A, postlysosomal compartments, the Golgi-complex, and mitochondria by confocal laser scanning microscopy. (A and A′) Anti-vacuolin antibody 221-1-1 was used to stain a postlysosomal compartment that acquires endocytic markers shortly before exocytosis. Single confocal sections of anti-vacuolin antibody-labeled cells revealed a substantial increase in the number of vesicular structures per nucleus in *dym*A$^-$ cells (A′) compared with wild-type cells (A). In contrast to the uniform size of immunostained late endosomal compartments in wild-type cells, the accumulated structures in *dym*A$^-$ cells display a wider variety in size and shape and frequently appear reticular. (B) Confocal sections showing the colocalization (yellow) of dynamin A (Alexa488, green) and vacuolin (Cy3, red) in Ax2 cells expressing GFP–dynamin A. The large vacuolin-positive compartment shows prominent, punctate dynamin A staining (see also right cell in panel D). (C) Confocal sections showing the localization of GFP–dynamin A (Alexa488, green) and the Golgi apparatus as visualized with antibody 190-340-8 (Cy3, red). (D) Localization of GFP–dynamin A (Alexa488, green) in comparison to the distribution of mitochondria (Cy3, red). Mitochondria were labeled with mAb 70-100-1, directed against a mitochondrial porin from *D. discoideum*. Bar, 10 μm. Magnification in panel A is identical to A′.

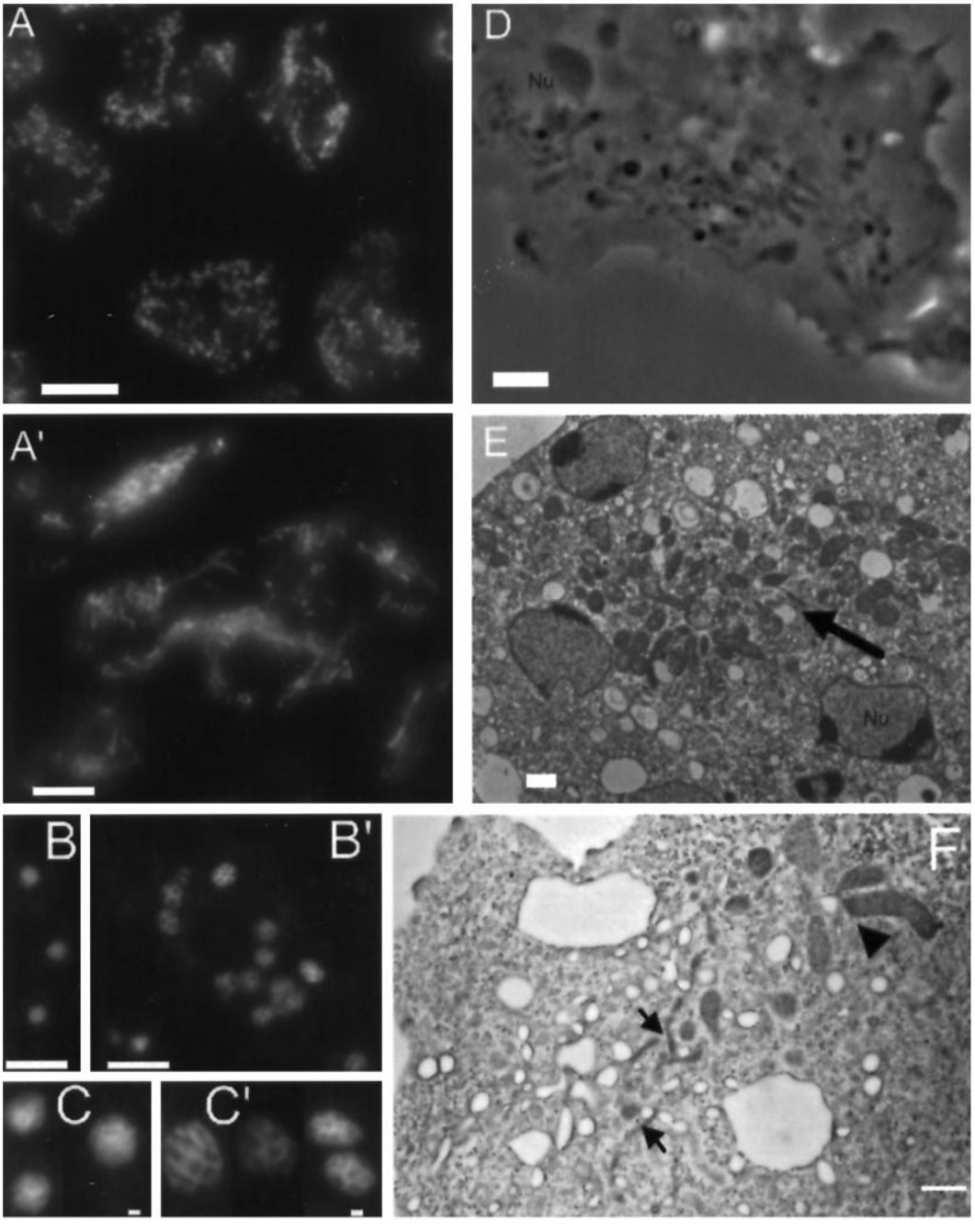

Figure 12. Cells lacking a functional copy of *dym*A become multinucleated and display abnormal morphologies of nuclei and mitochondria. Panels A and A′ show cells stained with mAb 70-100-1 directed against a mitochondrial porin from *D. discoideum*. (A) Uniform, dispersed appearance of mitochondria in Ax2 cells. (A′) In *dym*A$^-$ cells dense clusters of mitochondria are frequently observed, and most mitochondria appear fused in a network of long threads. (B) Ax2 cells were stained with DAPI to visualize nuclei. (B′) DAPI staining of Dynamin A-depleted cells shows that these cells are multinucleated. Panels C and C′ show a gallery of DAPI-stained nuclei. In comparison to wild-type nuclei (C), *dym*A$^-$ nuclei (C′) display a lobed appearance and are more variable in size and shape. (D) The altered appearance of mitochondria in *dym*A$^-$ cells can also be observed in phase contrast images. (E) EM micrographs showing clustered mitochondria (arrow) in a *dym*A$^-$ cell. (F) EM micrographs showing a branched mitochondrial network consisting of thin filamentous structures (arrows) and large lobe-shaped structures (arrowhead) in *dym*A$^-$ cells. Bar, 10 μm in panels A, A′, B, and B′, and 1 μm in panels C, C′, D, E, and F.

of vesicles from membranous structures and vesicle scission (Hinshaw and Schmid, 1995; Takei *et al.*, 1995). The absence of coated pits from the plasma membrane and the prominent and frequent occurrence of coated pit-decorated vesicles (Figure 10D) support the hypothesis that, in *D. discoideum*, fluid-phase uptake is an actin-dependent process and that dynamins play a role in the breakdown of macropinosomes and endosomes rather than the direct entry of extracellular fluid (Aubry *et al.*, 1997).

Pleiotropic effects of *shibire* and dynamin-1 mutations are well known (Poodry *et al.*, 1973; Chen *et al.*, 1991; van der Bliek *et al.*, 1993). Depletion of the closely related yeast Dnm1p, which, like dynamin A and DLP1, is mostly cytosolic, results in a twofold delay in the transport of endocytic material to the vacuole (Gammie *et al.*, 1995). However, recent studies provide strong evidence that Dnm1p localizes to the tip of mitochondria and functions primarily in the maintenance of yeast mitochondrial network morphology (Shaw *et al.*, 1997). Functions unrelated to vesicle trafficking have also been reported for the dynamin-like yeast proteins, Vps1p/Spo15p and Mgm1p. Vps1p/Spo15p is required for the timely separation of spindle-pole bodies in meiosis (Yeh *et al.*, 1991), while Mgm1p is needed for the maintenance of the mitochondrial genome (Jones and Fangman, 1992; Guan *et al.*, 1993), respectively. Our findings imply that dynamin A is likely to function in vesicle-trafficking processes related to the endo-lysosomal system of *D. discoideum.* The observed alterations in mitochondrial and nuclear morphology on dynamin A depletion are probably indirect consequences of a more general defect in membrane transport processes. This view is supported by the morphological alterations of the postlysosomal compartment in *dym*A$^-$ cells (Figure 9), a strong increase in the number of coated structures decorating intracellular membrane compartments in *dym*A$^-$ cells (Figure 10), and the finding that GFP-labeled dynamin A colocalizes mostly with vacuolin-decorated membranes and does not colocalize with either nuclei or mitochondria (Figure 11).

Further investigations will be greatly facilitated by the fact that *D. discoideum* is readily accessible by biochemical, cell biological, and molecular genetic approaches. This will help to clarify the involvement of dynamin A in cytokinesis and define the exact role of the protein in vesicle targeting and transport processes.

Accession Numbers

Dynamin A sequences reported in this article have been submitted to the GenBank/EMBL data bank with the accession numbers Q94464 for the peptide sequence and X99669 for the nucleotide sequence.

ACKNOWLEDGMENTS

We thank R. Albrecht, R. Batra, C. Heizer, E. Hirst, D. Hunt, R. Neujahr, M.D. Peterson, J. Sabry, S. Sinda, and I. Weber for help and advice; and J.A. Cardelli and co-workers for help with the secretion assays. We are especially grateful to G. Gerisch, H. Horstmann, M. Maniak, M. Sheetz, T. Soldati, and M. Titus for their many ideas and discussions. G. Gerisch, M. Maniak and A. Noegel provided antibodies 70-100-1, 221-1-1, and 190-340-8. We thank K.C. Holmes and W. Almers for support and encouragement. The work was supported by the Max Planck Society (Germany). M.L.W.K. was supported by a long-term fellowship from the European Molecular Biology Organization.

REFERENCES

Adessi, C., Chapel, A., Vincon, M., Rabilloud, T., Klein, G., Satre, M. and Garin, J. (1995). Identification of major proteins associated with *Dictyostelium discoideum* endocytic vesicles. J. Cell Sci. *108*, 3331–3337.

Aubry, L., Klein, G., and Satre, M. (1997). Cytoskeletal dependence and modulation of endocytosis in *Dictyostelium discoideum* amoebae. In: *Dictyostelium* a Model System for Cell and Developmental Biology, ed. Y. Maeda, K. Inouye, and I Takeuchi, Tokyo: Universal Academy Press, 65–72.

Bacon, R.A., Cohen, C.J., Lewin, D.A., and Mellman, I. (1994). Dictyostelium discoideum mutants with temperature-sensitive defects in endocytosis. J. Cell Biol. *127*, 387–399.

Bourne, H.R., Sanders, D.A., and McCormick, F. (1991). The GTPase superfamily: conserved structure and molecular mechanism. Nature *349*, 117–127.

Buczynski, G., Bush, J., Zhang, L., Rodriguez-Paris, J., and Cardelli, J.A. (1997). Evidence for a recycling role of Rab7 in regulating a late step in endocytosis and in retention of lysosomal enzymes in *Dictyostelium discoideum*. Mol. Biol. Cell *8*, 1343–1360.

Burki, E., Anjard, C., Scholder, J.C., and Reymond, C.D. (1991). Isolation of 2 genes encoding putative protein-kinases regulated during *Dictyostelium-discoideum* development. Gene *102*, 57–65.

Chen, M.S., Obar, R.A., Schroeder, C.C., Austin, T.W., Poodry, C.A., Wadsworth, S.C., and Vallee, R.B. (1991). Multiple forms of dynamin are encoded by *shibire*, a *Drosophila* gene involved in endocytosis. Nature *351*, 583–586.

Damke, H., Baba, T., van der Bliek, A.M., and Schmid, S.L. (1995). Clathrin-independent pinocytosis is induced in cells overexpressing a temperature-sensitive mutant of dynamin. J. Cell Biol. *131*, 69–80.

Damke, H., Baba, T., Warnock, D.E., and Schmid, S.L. (1994). Induction of mutant dynamin specifically blocks endocytic coated vesicle formation. J. Cell Biol. *127*, 915–934.

De Hostos, E.L., Bradtke, B., Lottspeich, F., Guggenheim, R., and Gerisch, G. (1991). Coronin, an actin binding protein of *Dictyostelium discoideum* localized to cell surface projections, has sequence similarities to G protein beta subunits. EMBO J. *10*, 4097–4104.

De Lozanne, A., and Spudich, J.A. (1987). Disruption of the *Dictyostelium* myosin heavy-chain gene by homologous recombination. Science *236*, 1086–1091.

Faix, J., Gerisch, G., and Noegel, A.A. (1992). Overexpression of the csA cell adhesion molecule under its own cAMP-regulated promoter impairs morphogenesis in *Dictyostelium*. J. Cell Sci. *102*, 203–214.

Fok, A.K., Clarke, M., Ma, L., and Allen, R.D. (1993). Vacuolar H(+)-ATPase of *Dictyostelium discoideum*. A monoclonal antibody study. J. Cell Sci. *106*, 1103–1113.

Gammie, A.E., Kurihara, L.J., Vallee, R.B., and Rose, M.D. (1995). DNM1, a dynamin-related gene, participates in endosomal trafficking in yeast. J. Cell Biol. *130*, 553–566.

Gamper, M., Howard, P.K., Hunter, T., and Firtel, R.A. (1996). Multiple roles of the novel protein tyrosine phosphatase PTP3 during *Dictyostelium* growth and development. Mol. Cell. Biol. *16*, 2431–2444.

Gu, X., and Verma, D.P. (1996). Phragmoplastin, a dynamin-like protein associated with cell plate formation in plants. EMBO J. *15*, 695–704.

Guan, K., Farh, L., Marshall, T.K., and Deschenes, R.J. (1993). Normal mitochondrial structure and genome maintenance in yeast requires the dynamin-like product of the *MGM*1 gene. Curr. Genet. *24*, 141–148.

Hacker, U., Albrecht, R., and Maniak, M. (1997). Fluid-phase uptake by macropinocytosis in *Dictyostelium*. J. Cell Sci. *110*, 105–112.

Heim, R., Cubitt, A.B., and Tsien, R.Y. (1995). Improved green fluorescence. Nature *373*, 663–664.

Heimer, G.V., and Taylor, C.E. (1974). Improved mountant for immunofluorescence preparations. J. Clin. Pathol. *27*, 254–256.

Herskovits, J.S., Burgess, C.C., Obar, R.A., and Vallee, R.B. (1993). Effects of mutant rat dynamin on endocytosis. J. Cell Biol. *122*, 565–578.

Hinshaw, J.E., and Schmid, S.L. (1995). Dynamin self-assembles into rings suggesting a mechanism for coated vesicle budding. Nature *374*, 190–192.

Jones, B.A., and Fangman, W.L. (1992). Mitochondrial DNA maintenance in yeast requires a protein containing a region related to the GTP-binding domain of dynamin. Genes & Dev. *6*, 380–389.

Kosaka, T., and Ikeda, K. (1983a). Possible temperature-dependent blockage of synaptic vesicle recycling induced by a single gene mutation in *Drosophila*. J. Neurobiol. *14*, 207–225.

Kosaka, T., and Ikeda, K. (1983b). Reversible blockage of membrane retrieval and endocytosis in the garland cell of the temperature-sensitive mutant of *Drosophila melanogaster*, shibirets1. J. Cell Biol. *97*, 499–507.

Kuwayama, H., Ecke, M., Gerisch, G., and Van Haastert, P.J. (1996). Protection against osmotic stress by cGMP-mediated myosin phosphorylation. Science *271*, 207–209.

Lamaze, C., and Schmid, S.L. (1995). The emergence of clathrin-independent pinocytic pathways. Curr. Opin. Cell Biol. *7*, 573–580.

Liu, T., Williams, J.G., and Clarke, M. (1992). Inducible expression of calmodulin antisense RNA in *Dictyostelium* cells inhibits the completion of cytokinesis. Mol. Biol. Cell *3*, 1403–1413.

Maniak, M., Rauchenberger, R., Albrecht, R., Murphy, J., and Gerisch (1995). Coronin involved in phagocytosis: dynamics of particle-induced relocalization visualized by a green fluorescent protein Tag. Cell *83*, 915–924.

Mann, S.K., and Firtel, R.A. (1991). A developmentally regulated, putative serine/threonine protein kinase is essential for development in *Dictyostelium.* Mech. Dev. *35*, 89–101.

Manstein, D.J., Schuster, H.-P., Morandini, P., and Hunt, D.M. (1995). Cloning vectors for the production of proteins in *Dictyostelium discoideum*. Gene *162*, 129–134.

Manstein, D.J., Titus, M.A., De Lozanne, A., and Spudich, J.A. (1989). Gene replacement in *Dictyostelium*: generation of myosin null mutants. EMBO J. *8*, 923–932.

Morré, D.J., Brightman, A.O., and Sandelius, A.S. (1987). In: Biological Membranes: A Practical Approach, ed. J.B.C. Findlay and W.H. Evans, Oxford, England: IRL Press, 37–50.

Muhlberg A.B., Warnock D.E., and Schmid S.L. (1997). Domain structure and intramolecular regulation of dynamin GTPase. EMBO J. *16*, 6676–6683.

Neuhaus, E.M., Horstmann, H., Almers, W., Maniak, M., and Soldati, T. (1998). Ethane-freezing/methanol-fixation of cell monolayers—a procedure for improved preservation of structure and antigenicity for light and electron microscopies. J. Struct. Biol. *121*, 326–342.

Neujahr R., Heizer, C., and Gerisch, G. (1997). Myosin II-independent processes in mitotic cells of *Dictyostelium discoideum*: redistribution of the nuclei, re-arrangement of the actin system and formation of the cleavage furrow. J. Cell Sci. *110*, 123–137.

Niswonger, M.L., and O'Halloran T.J. (1997a). A novel role for clathrin in cytokinesis. Proc. Natl. Acad. Sci. USA *94*, 8575–8578.

Niswonger, M.L., and O'Halloran, T.J. (1997b). Clathrin heavy chain is required for spore cell but not stalk cell differentiation in *Dictyostelium discoideum*. Development *124*, 443–451.

Nothwehr, S.F., Conibear, E., and Stevens, T.H. (1995). Golgi and vacuolar membrane proteins reach the vacuole in *vps1* mutant yeast cells via the plasma membrane. J. Cell Biol. *129*, 35–46.

Novak, K.D., Peterson, M.D., Reedy, M.C., and Titus, M.A. (1995). Dictyostelium myosin I double mutants exhibit conditional defects in pinocytosis. J. Cell Biol. *131*, 1205–1221.

Obar, R.A., Collins, C.A., Hammarback, J.A., Shpetner, H.S., and Vallee, R.B. (1990). Molecular cloning of the microtubule-associated mechanochemical enzyme dynamin reveals homology with a new family of GTP-binding proteins. Nature *347*, 256–261.

O'Halloran, T.J., and Anderson, R.G. (1992). Characterization of the clathrin heavy chain from *Dictyostelium discoideum*. DNA Cell Biol. *11*, 321–330.

Park, J.M., Cho, J.H., Kang, S.G., Jang, H.J., Pih, K.T., Piao, H.L., Cho, M.J., and Hwang, I. (1998). A dynamin-like protein in *Arabidopsis thaliana* is involved in biogenesis of thylakoid membranes. EMBO J. *17*, 859–867.

Poodry, C.A., Hall, L., and Suzuki, D.T. (1973). Developmental properties of *shibire*: a pleiotropic mutation affecting larval and adult locomotion and development. Dev. Biol. *32*, 373–386.

Raper, K.B. (1935). *Dictyostelium discoideum*, a new species of slime mold from decaying forest leaves. J. Agric. Res. *58*, 135–147.

Rauchenberger, R., Hacker, U., Murphy, J., Niewohner, J., and Maniak, M. (1997). Coronin and vacuolin identify consecutive stages of a late, actin-coated endocytic compartment in *Dictyostelium*. Curr. Biol. *7*, 215–218.

Ruscetti, T., Cardelli, J.A., Niswonger, M.L., and O'Halloran, T.J. (1994). Clathrin heavy chain functions in sorting and secretion of lysosomal enzymes in *Dictyostelium discoideum*. J. Cell Biol. *126*, 343–352.

Sambrook, J., Fritsch, E.F., and Maniatis, T. (1989). Molecular Cloning: A Laboratory Manual, 2nd ed., Cold Spring Harbor, NY: Cold Spring Harbor Laboratory Press.

Shaw, J.M., Otsuga, D., Keegan, B., Hermann, G., and Bleazard, W. (1997). The dynamin-like GTPase Dnm1p is required for maintenance of yeast mitochondrial network morphology. Mol. Biol. Cell *8*, 2470a (Abstract).

Shin, H.W., Shinotsuka, C., Torii, S., Murakami, K., and Nakayama, K. (1997). Identification and subcellular localization of a novel mammalian dynamin-related protein homologous to yeast Vps1p and Dnm1p. J. Biochem. *122*, 525–530.

Stott, K., Blackburn, J.M., Butler, P.J.G., and Perutz, M. (1995). Incorporation of glutamine repeats makes protein oligomerize: implications for neurodegenerative diseases. Proc. Natl. Acad. Sci. USA *92*, 6509–6513.

Sutoh, K. (1993). A transformation vector for *Dictyostelium discoideum* with a new selectable marker bsr. Plasmid. *30*, 150–154.

Takei, K., McPherson, P.S., Schmid, S.L., and De Camilli, P. (1995). Tubular membrane invaginations coated by dynamin rings are induced by GTP-γ-S in nerve terminals. Nature *374*, 186–190.

Temesvari, L.A., Bush, J.M., Peterson, M.D., Novak, K.D., Titus, M.A., and Cardelli, J.A. (1996). Examination of the endosomal and lysosomal pathways in *Dictyostelium discoideum* myosin I mutants. J. Cell Sci. *109*, 663–673.

Troll, H., Malchow, D., Muller-Taubenberger, A., Humbel, B., Lottspeich, F., Ecke, M., Gerisch, G., Schmid, A., and Benz, R. (1992). Purification, functional characterization, and cDNA sequencing of mitochondrial porin from *Dictyostelium discoideum*. J. Biol. Chem. *267*, 21072–21079.

Urrutia, R., Henley, J.R., Cook, T., and McNiven, M.A. (1997). The dynamins: redundant or distinct functions for an expanding family of related GTPases? Proc. Natl. Acad. Sci. USA *94*, 377–384.

van der Bliek, A.M., and Meyerowitz, E.M. (1991). Dynamin-like protein encoded by *Drosophila* shibire gene associated with vesicular traffic. Nature *351*, 411–414.

van der Bliek, A.M., Redelmeier, T.E., Damke, H., Tisdale, E.J., Meyerowitz, E.M., and Schmid, S.L. (1993). Mutations in human dynamin block an intermediate stage in coated vesicle formation. J. Cell Biol. *122*, 553–563.

Varnum B., Edwards K.B., and Soll D.R. (1985). *Dictyostelium* amebae alter motility differently in response to increasing versus decreasing temporal gradients of cAMP. J. Cell Biol. *101*, 1–5.

Vater, C.A., Raymond, C.K., Ekena, K., Howald-Stevenson, I., and Stevens, T.H. (1992). The VPS1 protein, a homolog of dynamin required for vacuolar protein sorting in *Saccharomyces cerevisiae*, is a GTPase with two functionally separable domains. J. Cell Biol. *119*, 773–786.

Weiner, O.H., Murphy, J., Griffiths, G., Schleicher, M., and Noegel, A. (1993). The actin-binding protein comitin (p24) is a component of the Golgi apparatus. J. Cell Biol. *123*, 23–34.

Westphal, M., Jungbluth, A., Heidecker, M., Muhlbauer, B., Heizer C., Schwartz, J.M., Marriott, G., and Gerisch, G. (1997). Microfilament dynamics during cell movement and chemotaxis monitored using a GFP-actin fusion protein. Curr. Biol. *7*, 176–183.

Wienke, D.C., Batra, R., Knetsch, M.L.W., and Manstein, D.J. (1997). Overexpression, purification and characterization of a *Dictyostelium* dynamin-homologue. Mol. Biol. Cell *8*, 2471a (Abstract).

Wilsbach, K., and Payne, G.S. (1993). Vps1p, a member of the dynamin GTPase family, is necessary for Golgi membrane protein retention in *Saccharomyces cerevisiae*. EMBO J. *12*, 3049–3059.

Yeh, E., Driscoll, R., Coltrera, M., Olins, A., and Bloom, K. (1991). A dynamin-like protein encoded by the yeast-like sporulation gene *SPO15*. Nature *349*, 713–715.

Yoon, Y., Pitts, K.R., Dahan, S., and McNiven, M.A. (1998). A novel dynamin-like protein associates with cytoplasmic vesicles and tubules of the endoplasmic reticulum in mammalian cells. J. Cell Biol. *140*, 779–793.

Zhu, Q., Liu, T., and Clarke, M. (1993). Calmodulin and the contractile vacuole complex in mitotic cells of *Dictyostelium discoideum*. J. Cell Sci. *104*, 1119–1127.